

1 **Relevance of acoustic methods to quantify bedload transport** 2 **and bedform dynamics in a large sandy-gravel bed river**

3 Jules Le Guern¹, Stéphane Rodrigues^{1,2}, Thomas Geay³, Sébastien Zanker⁴, Alexandre Hauet⁴,
4 Pablo Tassi^{5,6}, Nicolas Claude^{5,8}, Philippe Jugé⁷, Antoine Duperray¹, Louis Vervynck¹.

5 ¹UMR CNRS CITERES, University of Tours, France.

6 ²Graduate School of Engineering Polytech Tours, University of Tours, France.

7 ³BURGEAP R&D, Grenoble, France.

8 ⁴EDF, Division Technique Générale, Grenoble, France.

9 ⁵EDF R&D – National Laboratory for Hydraulics and Environment (LNHE), Chatou, France.

10 ⁶Saint-Venant Laboratory for Hydraulics, Chatou, France.

11 ⁷CETU Elmis Ingénieries, University of Tours, Chinon, France.

12 ⁸EDF, Centre Ingénierie Hydraulique, La Motte Servolex, France.

13 *Correspondence to:* Jules Le Guern (leguern@univ-tours.fr).

14 **Abstract**

15 **Despite the inherent difficulties to quantify its value, bedload transport is essential to understand fluvial**
16 **systems. In this study, we assessed different indirect bedload measurement techniques with a reference**
17 **direct bedload measurement in a reach of a large sandy-gravel bed river. Acoustic Doppler Current Profiler**
18 **(aDcp), Dune Tracking Method (DTM) and hydrophone measurement techniques were used to determine**
19 **bedload transport rates by using calibration with the reference method or by using empirical formulas.**
20 **Results show that the hydrophone is the most efficient and accurate method to determine bedload fluxes**
21 **in the Loire River. Although further work is needed to identify the parameters controlling sediment self-**
22 **generated noise, the calibration procedure adopted in this study allows a satisfactory estimation of**
23 **bedload transport rates. Moreover, aDcp and hydrophone measurement techniques are accurate enough**
24 **to quantify bedload variations associated to dune migration.**

25 **1. Introduction**

26 Worldwide, rivers are in crisis (Vörösmarty et al., 2010). While changes in flow characteristics and fragmentation
27 are well known (Grill et al., 2019), the impacts of human activities on the sediment budgets are yet
28 underrepresented (Kondolf et al., 2018). The quantification of bedload transport is a key element to understand,
29 manage and restore the physical and ecological functioning of fluvial systems. It is a prerequisite to an accurate
30 estimation of global sediment budgets delivered by rivers to oceans (Syvitski and Milliman, 2007), to better
31 understand bedform dynamics in river channels (Best, 1988; Bertoldi et al., 2009; Rodrigues et al., 2015; Claude

32 et al., 2014) and to reproduce satisfactorily morphodynamic processes with numerical modelling (Mendoza et al.
33 2017; Cordier et al., 2020).

34 However, in large rivers, this parameter remains difficult to estimate mainly due to human and material resources
35 required to collect accurate measurements. Among the available tools, indirect measurement techniques are
36 promising alternatives to direct measurements that are often cumbersome to implement, and can be time-
37 consuming and perilous (Gray et al., 2010). Since the 2000s, numerous studies were proposed to process the
38 signal captured by acoustic Doppler current profilers (aDcp) as a tool for determining the apparent bedload velocity
39 (Rennie et al., 2002; Rennie and Villard, 2004; Rennie and Millar, 2004; Kostaschuk et al., 2005; Villard et al.,
40 2005; Gaeuman and Jacobson 2006; 2007; Holmes et al., 2010; Ramoos and Rennie, 2010; Latosinski et al., 2017;
41 Conevski et al., 2019; Conevski et al., 2020a). The use of passive acoustic instruments has also been widely used
42 to quantify bedload transport. Even though these latter techniques have been developed through the application of
43 measurement tools such as geophones or hydrophones, their domain of applicability is restricted to the study of
44 rivers with coarse sediments (Barton et al., 2010; Hildale et al., 2014; Marineau et al., 2016; Geay et al., 2017).
45 In sandy-gravel bed rivers, the presence of bedforms is generally used to indirectly estimate bedload transport
46 (Simons et al., 1965). Single beam (Peters, 1978; Engel and Lau, 1980) or multibeam echosounders (Nittrouer et
47 al., 2008; Leary and Buscombe, 2020) are techniques tools usually adopted to determine morphological parameters
48 (such as bedform height, wavelength and celerity) or to estimate sediment budget (Frings et al., 2014). These
49 bathymetrical surveys are often carried out simultaneously with sediment sampler measurements (Gaeuman and
50 Jacobson, 2007; Claude et al., 2012) to calibrate the signal with a direct reference although the latter are intrusive
51 and characterized by a low spatial representativeness. These drawbacks can therefore limit the applicability of
52 these measurement techniques, in particular for large lowland rivers.

53 In this work, we compare the efficiency of active and passive acoustic techniques to quantify bedload transport.
54 The investigation took place in a reach of the Loire River (France), which is characterized by the presence of
55 migrating bars and superimposed dunes (Le Guern et al., 2019b).

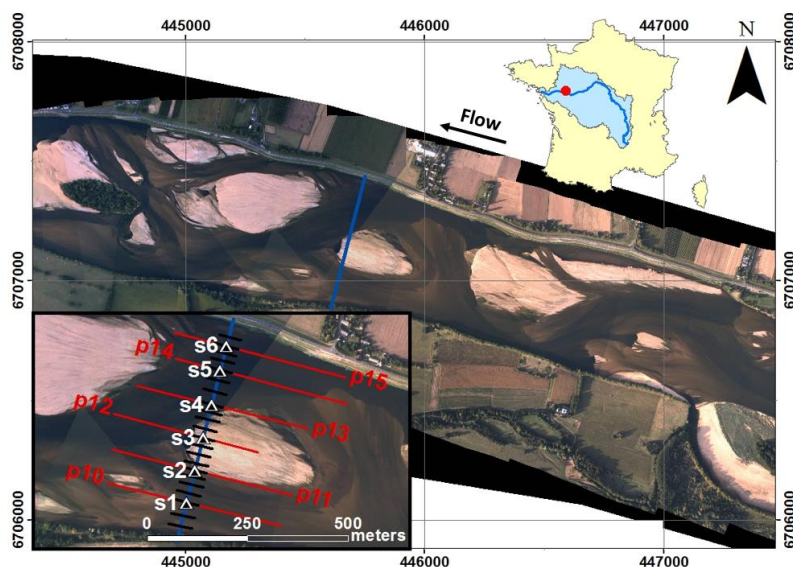
56 The main objectives of this study were: 1) to compare indirect methods for estimating bedload with bedload
57 estimates based on physical samples; 2) to estimate the accuracy of acoustic methods to measure cross sectional
58 variations of bedload fluxes for various discharge conditions; and 3) to investigate the capabilities of hydrophones
59 and aDcps at capturing bedload variations along bedforms.

60 **2. Study site**

61 The study site is located near Saint-Mathurin-sur-Loire, in the lower reach of the Loire River (France), approximately
62 150 km upstream of the mouth of the Loire River. The study reach is 2.5 km long, 500 m wide, nearly straight, with
63 a bed slope of 0.02 % (Fig. 1). The riverbed is composed of a mixture of siliceous sands and gravels with a median

64 diameter (D_{50}) of 0.9 mm. It varies between 0.3 and 3.1 mm with a standard deviation of 0.4 mm. The 90th percentile
65 of the sediment grain size distribution (D_{90}) is variable with a median value of 3.3 mm varying from 0.5 to 15.7 mm.
66 Hydraulic conditions at the sampling points varied with discharge and the median water depth and water velocity
67 are 1.6 m and 0.9 m.s⁻¹ respectively. The width-to-depth ratio ranges from 120 to 550 depending on discharge
68 variations. The mean annual discharge at the Saumur gauging station (approx. 30 km upstream) is 680 m³.s⁻¹, with
69 a 2-years flood of 2700 m³.s⁻¹. Surveys were conducted during various hydrological conditions, with flow discharges
70 ranging from 200 to 2400 m³.s⁻¹ (Fig. 2a).

71 Bars are characterized by an average wavelength of 1300 m, corresponding to approximately three times the
72 channel width. The mean bar height is 1.5 m. At submerged conditions, bars can migrate with a celerity of 0.5 to 2
73 meters per day. During floods, the bar celerity can increase up to 4 meters per day (Le Guern et al., 2019a). During
74 floods, dunes are superimposed to bars, whose height, wavelength and mean celerity are approximately of 0.3 m,
75 4.4 m and 32 meters per day, respectively.

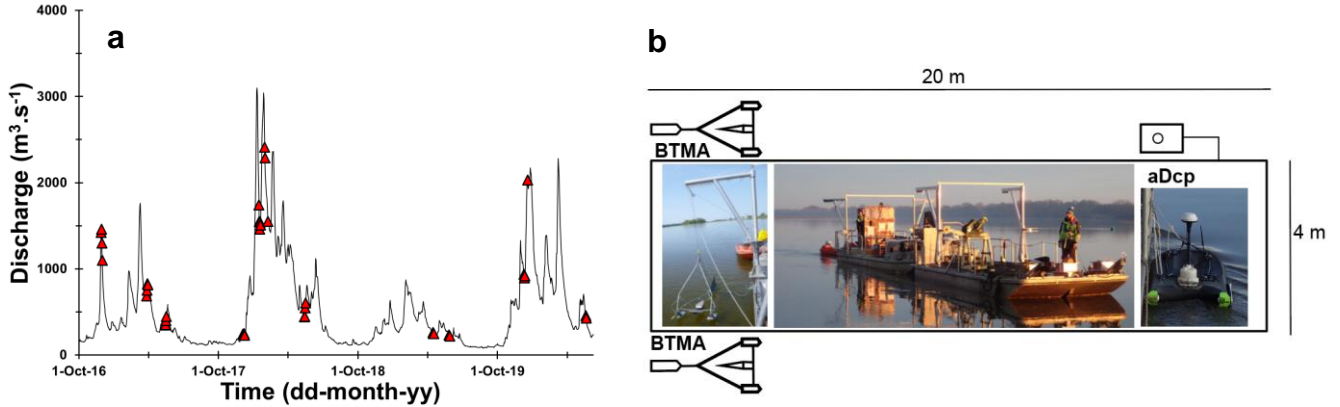


76
77 **Fig. 1: Aerial photographs of the study site in 2017 (courtesy of Dimitri Lague, University of Rennes, France) with**
78 **location of sampling points (white triangles) on the sediment transport gauging cross section (blue line), bathymetric**
79 **profiles (red lines) and hydrophone drifts (black lines).**

80 **3. Materials and methods**

81 Direct measurements of bedload sediment transport rates were performed using pressure- difference samplers.
82 This conventional approach was used to evaluate three indirect acoustic methods: the apparent bedload velocity
83 assessed from aDcp measurements, the dune tracking method (DTM) inferred using single-beam echosounding,
84 and the self-generated noise (SGN) of sediments measured using a hydrophone. A total of 72 surveys were

85 performed from October 2016 to May 2020 (discharge ranging between 210 m³.s⁻¹ and 2290 m³.s⁻¹) including 43
 86 surveys with isokinetic samplers presented on Fig. 2a.



87
 88 **Fig. 2: (a), distribution of surveys along the hydrograph of Saumur gauging station located about 30 km upstream the**
 89 **study site. (b), Scheme of the main boat and disposition of monitoring facilities.**

90 3.1. Bedload rates obtained using isokinetic samplers

91 Bedload transport rates were measured using two synchronized Bedload Transport Meter Arnheim (BTMA)
 92 samplers, consisting on a sampling basket mounted on a frame. The sampling basket have a rectangular mouth of
 93 0.05 m high and 0.085 m wide. Complete description of the sample can be found in de Vries (1979) or in Eijkelkamp
 94 (2003). Devices were mounted on a 20 meter-long boat stabilized using two anchors (Fig. 2b). These two samplers
 95 were deployed on 6 sampling points (S1 to S6) distributed along a cross section (Fig. 1). At each sampling point,
 96 10 samples were collected with each BTMA (20 in total) and volumes of each samples were measured *in situ* with
 97 a graduated cone (Imhoff cone). Collected volumes were integrated over at least 2 minutes. All samples volumes
 98 from each BTMA were merged for sieving analysis (leading to 2 sediment samples per sampling point; one for
 99 each BTMA). Then, the average volume of caught sediments from the 2 BTMAs was computed and converted into
 100 instantaneous unit bedload rates as follow:

$$101 \quad q_{sBTMA} = \frac{V}{b} \alpha \varepsilon \rho_s \times 10^3; \quad (1)$$

102 where q_{sBTMA} is the unit bedload transport rate (g.s⁻¹.m⁻¹), α is the trap efficiency factor based on calibration ($\alpha=2$),
 103 V is the mean volume of the instantaneous sediment catch (m³.s⁻¹), b is instrument's mouth width ($b=0.085$ m), ρ_s
 104 is the sediment density (2650 kg.m⁻³) and ε is the volumetric sediment concentration (assumed to be equal to 0.65).
 105 Suggested values of α and b were adopted from Boiten (2003) which mentioned that the trap efficiency factor not
 106 include the possible losses of sediment finer than 0.3 mm (mesh size opening). Sampler positions and sampling
 107 quality were controlled by using two cameras mounted on the BTMAs but records during flood events were
 108 unusable because of increasing water depth and suspension. Sediment samples were analysed using the standard
 109 sieving technique (Folk and Ward, 1957) to determine the grain size distribution (GSD) using the tool "GRADISTAT"

110 developed by Blott and Pye (2001). Uncertainties associated to the estimation of the unit bedload were calculated
 111 following Frings and Vollmer (2017).

112 3.2. Apparent bedload velocity from aDcp

113 Simultaneously with the BTMA measurements, an aDcp was installed on the boat (Fig. 2b). Measurements were
 114 performed using a Sontek Riversurveyor M9 (bi-frequency, 1 and 3 MHz) or a Teledyne RD Instruments Rio Grande
 115 (1.2 MHz). The sampling time needed to get a stable apparent velocity is in the range 3 min for the case without
 116 bedforms (Conevski et al., 2019) and 25 min (Rennie et al., 2002). In our study the sampling time range was
 117 between 5 and 190 minutes. The aDcp was coupled with a RTK GPS Magellan ProFlex 500 receiving position
 118 corrections via the Teria network (centimeter level accuracy). The aDcp measurement allowed the use of both
 119 empirical approach and calibration approach for comparison with sediment sampler measurements. The apparent
 120 bedload velocity V_a was estimated from the bottom tracking signal, allowing the identification and the position of
 121 the river bed. In case of mobile bed, the Doppler shift of the backscattered acoustic pulse of the bottom track
 122 depends on to the boat velocity and to the bed velocity. According to Rennie et al. (2002), the apparent bedload
 123 velocity can be estimated using:

$$124 \quad V_a = V_{GPS} - V_{BT}; \quad (2)$$

125 where V_{GPS} and V_{BT} are the boat velocity according to GPS reference and bottom track respectively. When the
 126 GPS signal was poor or missing, the apparent velocity was considered to be equal to the boat velocity according
 127 to bottom track reference because measurements were performed in a static position (representing 15% of the
 128 dataset). Following Jamieson et al. (2011), the apparent velocity V_a was calculated for the North and East velocity
 129 components (respectively \vec{V}_{aE} and \vec{V}_{aN}), limiting the over estimation especially in areas where inconsistent

$$130 \quad \text{directions and low magnitudes of bedload velocity were found: } V_a = \sqrt{V_{aE}^2 + V_{aN}^2}.$$

131 To avoid compass and GPS issues, and to eliminate the effect of residual lateral displacement of the anchored
 132 boat, the apparent bedload velocity was projected onto the flow direction using:

$$133 \quad V_{a\text{proj}} = V_a \cdot \cos\left(\frac{w_{dir\ BT} - b_{dir\ BT}}{180} \cdot \pi\right); \quad (3)$$

134 with $w_{dir\ BT}$ the flow direction with bottom track reference and $b_{dir\ BT}$ the boat direction with the bottom track reference
 135 (in degree). Equation (3) gives a value of apparent bedload transport velocity for each time step (approximately
 136 equal to 1 s) that was averaged to obtain a value for each sampling point. This method assumes that bedload is
 137 orientated in the same direction than the main flow. According to Rennie et al. (2002), the bedload transport rate
 138 per unit width ($q_s\ ADCP$, $\text{g}\cdot\text{s}^{-1}\cdot\text{m}^{-1}$) can be computed from two different kinematic models, namely:

$$139 \quad q_s\ ADCP = \frac{4}{3} \rho_s r V_{a\text{proj}} \times 10^3; \quad (4)$$

140 where $r = D_{50}/2$ is the particle radius, D_{50} is the median sediment diameter (m), ρ_s is the sediment density (2650
 141 kg.m⁻³). In this model, it is assumed the maximum bedload thickness is a single particle and:

$$142 \quad q_s ADCP = V_{a \text{ proj}} d_s c_b \rho_s; \quad (5)$$

143 where c_b is the concentration of the active transport layer considered as the saltation height (van Rijn, 1984), and
 144 the van Rijn (1984) formulation was adopted to compute the active layer thickness (d_s) as a function of the hydraulic
 145 condition and sediment grain size:

$$146 \quad d_s = 0.3 D_*^{0.7} T^{0.5} D_{50}; \quad (6)$$

$$147 \quad c_b = 0.18 \frac{T}{D_*} c_0; \quad (7)$$

$$148 \quad T = \frac{(u_*')^2 - (u_{*cr})^2}{(u_{*cr})^2}; \quad (8)$$

$$149 \quad u_*' = \frac{\bar{u}}{5.75 \log\left(\frac{12d}{3D_{90}}\right)}; \quad (9)$$

150 where c_0 is the maximum bedload concentration (0.65), T is the transport stage parameter that reflects the
 151 sediment mobility, u_*' is the bed shear velocity related to the grain (m.s⁻¹), d is the mean water depth (m), \bar{u} is the
 152 mean flow velocity measured from the aDcp (m.s⁻¹) and u_{*cr} is the critical bed shear velocity (m.s⁻¹) calculated from
 153 the Shields curve (Van Rijn, 1984) and function of grain size through the scaled particle parameter D_* :

$$154 \quad D_* = D_{50} \left[\frac{(s-1)g}{\nu^2} \right]^{\frac{1}{3}}; \quad (10)$$

155 where g is the acceleration of the gravity (m.s⁻²), ν is the kinematic viscosity (m².s⁻¹) and s the sediment density
 156 ratio. For the range of grain size of this study, u_{*cr} is computed as follows:

$$157 \quad 10 < D_* \leq 20; u_{*cr} = [0.04 D_*^{0.1} (s-1)gD_{50}]^{0.5}; \quad (11)$$

$$158 \quad 20 < D_* \leq 150; u_{*cr} = [0.013 D_*^{0.29} (s-1)gD_{50}]^{0.5}; \quad (12)$$

159 In order to evaluate the sensibility of the apparent bedload post-processing, the two kinematic models (Eq. 4 and
 160 Eq. 5) were tested using raw apparent bedload velocity (V_a) and projected apparent bedload velocity ($V_{a \text{ proj}}$).

161 To assess the capability of the aDcp to detect bedforms through the evolution of apparent bedload velocity, 3
 162 surveys were conducted by positioning the aDcp 0.6 m above the river bed. This experimental scheme was adopted
 163 to avoid lateral movements of the boat, to be as close as possible to the river bed, and to reduce the space between
 164 beams. This configuration permitted to fix the footprint for each beam to about 0.0046 m² and a distance of 0.56 m
 165 between opposed beams. This allowed to describe the apparent bedload velocity with a finer accuracy especially
 166 in the presence of bedforms of 0.2 m height and 3.9 m long (in average). These surveys were performed for several
 167 hours (from 2.1 h to 4.7 h) to capture the migration of more than one dune lee side pass under the device. The
 168 value of apparent bedload velocity was smoothed by using a moving windows with an average of 500 points

169 (approximately 500 seconds) to remove the outliers from the raw dataset. In the present study, all negative values
170 were excluded from the comparison with BTMA measurements (16% of apparent velocity values).

171 3.3. Bathymetrical echosounding and dune tracking method

172 A single beam echosounder Tritech PA500 (0.5 kHz) coupled with a RTK GPS LEICA Viva GS25 were used for
173 high-frequency bathymetric surveys to determine bar and dune morphodynamics along 6 longitudinal profiles
174 (about 400 m long) centred on sampling points indicated in Fig. 1. Dune height (H_D) and wavelength (λ_D) were
175 estimated using the Bedform Tracking Tool (BTT) based on the zero-crossing method (Van der Mark and Blom,
176 2007). Dune celerity (C_D) was estimated with the Dune Tracking Method (DTM, Simons et al., 1965; Engel and
177 Lau, 1980) following the dune crests between two subsequent bathymetric surveys for a mean interval time equal
178 to 40 minutes. The interval time needs to be adjusted with discharge because of the dune celerity variation from
179 one survey to another. The determination of a proxy to evaluate sediment transport directly from DTM
180 measurements is difficult because dune migration is function of several parameters. A semi-empirical equation that
181 accounts for these parameters was used to compare bedload transport rates with the reference measurement. The
182 computed dune parameters were used to calculate the unit bedload transport rate (q_s^{DTM} , $\text{g.s}^{-1}.\text{m}^{-1}$) using the
183 formula by Simons et al. (1965):

$$184 \quad q_s^{DTM} = (1-\lambda) \rho_s H_D C_D \beta \times 10^3; \quad (13)$$

185 where H_D is the mean dune height along the profile (m), C_D is the median dune celerity (m.s^{-1}) and β is the bedload
186 discharge coefficient equal to 0.5 for a perfect triangular dune shape. The β coefficient neglects the volume of
187 bypassing material from previous dunes or exchanges between bedload and suspended load (Wilbers, 2004). Due
188 to its large variability (Van den Berg, 1987; Ten Brinke et al., 1999; Wilbers, 2004), the sensibility of the bedload
189 transport rate was assessed for $\beta=[0.33; 0.57]$, as proposed by Engel and Lau (1980) and Wilbers (2004).
190 Considering the accuracy of the bathymetrical echosounding relative to the dune size, the sinuosity of dune crests,
191 and the representativeness of dune celerity, only profiles with a mean dune height greater than 0.1 m and more
192 than 10 dunes were considered.

193 3.4. Hydrophone and acoustic power

194 Passive acoustic monitoring was performed with a Teledyne RESON Hydrophone TC4014-5 (sensitivity of -180
195 dB) plugged into an EA-SDA14 card from RTSYS Company. This device has a large frequency range from 0.015
196 to 480 kHz, with a linear response until 250 kHz ($\pm 3\text{dB}$). The beam-pattern of the hydrophone is omnidirectional.
197 The hydrophone has been deployed following the protocol proposed by Geay et al. (2020). Longitudinal profiles
198 were defined on the sediment transport sampling section (22 see Fig. 1). The boat was positioned upstream the
199 sediment transport gauging section and left adrift at flow velocity. Depending on the water depth, the hydrophone

200 was installed at a constant depth between 0.4 and 0.7 m below the water surface. Data acquisition was stopped
201 after the boat crossed the sediment transport gauging section. The drift duration ranged between 15 to 140
202 seconds, depending on the flow velocity (mean time of 31 s). For each drift, a spectral probability density (SPD)
203 was computed (Merchant et al., 2013). Then, a median Power Spectral Density (PSD) was computed as proposed
204 by Geay et al. (2017). Median PSD are preferred to mean PSD as it enables to filter anomalous acoustic events
205 such as the hydrophone impinging the riverbed. The acoustic power (P) for each drift was computed by integrating
206 the median PSD over a range of frequency comprised between f_{min} (15 kHz) and f_{max} (350 kHz) (Geay et al., 2020):

$$207 \quad P = \int_{f_{min}}^{f_{max}} PSD(f) df ; \quad (14)$$

208 The minimum frequency was chosen to avoid hydrodynamic and engine noises, while the maximum frequency was
209 set by the upper limit frequency of the device and was adjusted related to PSD . Finally, the nearest hydrophone
210 drift for each BTMA sampling point was selected. Hydrophone drifts and sampler measurements were not
211 synchronized. Several tests were carried out to ensure that these acoustic power variations were not related to the
212 distance between the hydrophone and the river bed. As no theoretical expression has been developed to estimate
213 bedload rates from hydrophone measurements, only the calibration approach was implemented.

214 4. Results

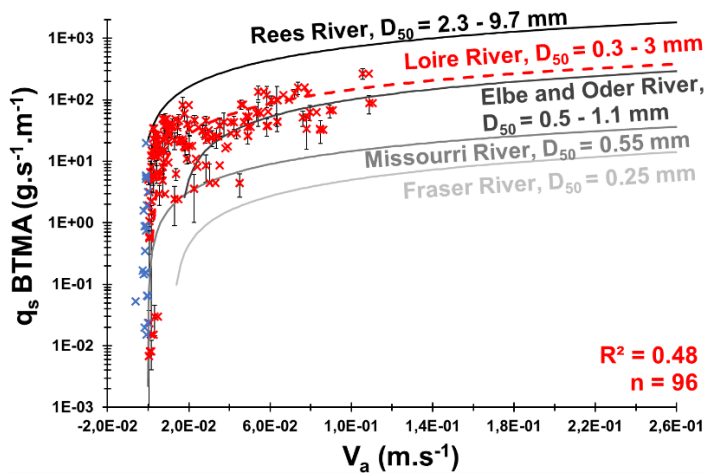
215 4.1. Comparison between acoustics and direct bedload transport rate measurements

216 The BTMA dataset is composed of 135 unit bedload rates calculated from 2628 individual sediment samples. This
217 dataset represents an average of 19 samples on each sampling point to compute unit bedload rates (minimum of
218 5 and maximum of 57 samples). Bedload rates measured using the BTMAs ranged between 0.01 and 268 $\text{g}\cdot\text{s}^{-1}\cdot\text{m}^{-1}$.
219 The standard deviation of unit bedload rates increased with discharge with a mean value of 33 $\text{g}\cdot\text{s}^{-1}\cdot\text{m}^{-1}$. This
220 illustrates the spatio-temporal variability of sediment transport induced by bedform migration.

221 The aDcp dataset is composed of 96 simultaneous measurements of apparent bedload velocity and BTMA
222 samplings (Fig. 3a). The mean apparent bedload velocity is 0.02 $\text{m}\cdot\text{s}^{-1}$ and the maximum value was 0.11 $\text{m}\cdot\text{s}^{-1}$. A
223 Reduced Major Axis (RMA) regression has been computed between these two variables with a coefficient of
224 determination (COD) R^2 equal to 0.51:

$$225 \quad q_s = 1456 V_a - 2.44 ; \quad (15)$$

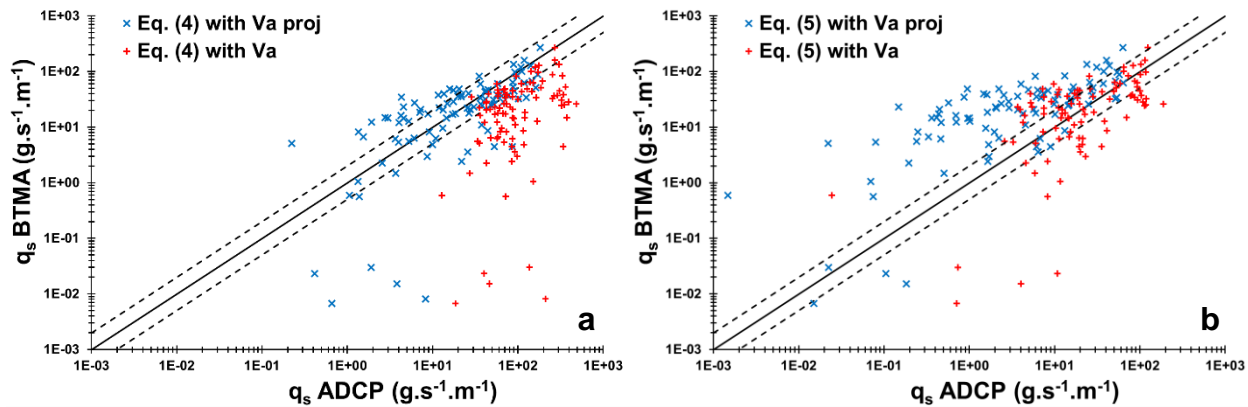
226 As shown in Fig. 3a, this site-specific calibration procedure at a reach of the Loire River describes fairly well the
227 dataset already published on several world large rivers (Rennie et al., 2017).



228

229 **Fig. 3: unit bedload transport rates measured with BTMA samplers as a function of the apparent bedload velocity**
 230 **measured with aDcp. Red dashed line represents the RMA regression of the Loire River. Comparison with other site-**
 231 **specific calibration curves (Conevski et al., 2020a; Rennie et al. 2017). Blue marks represent negatives apparent**
 232 **bedload velocity excluded from this regression.**

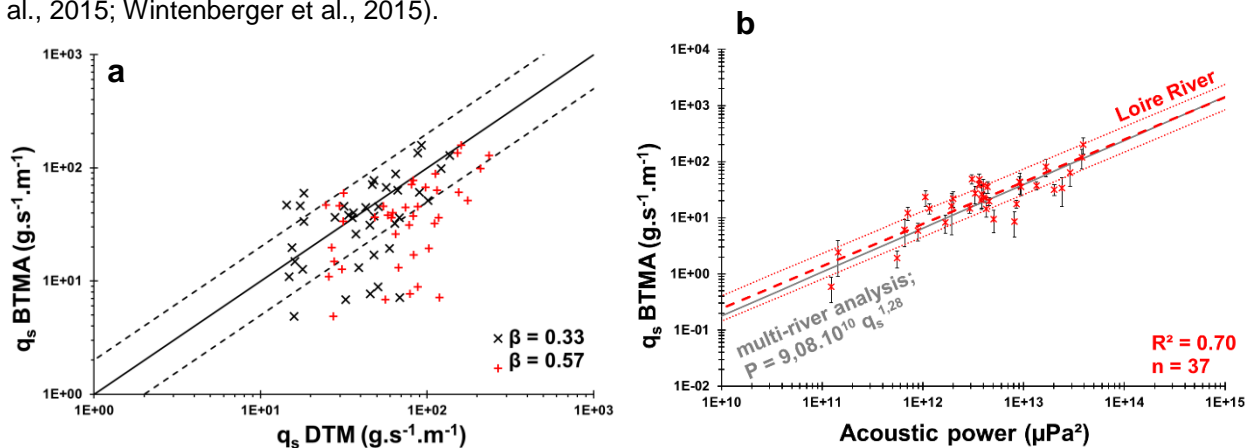
233 To evaluate the accuracy of a method against a reference, the discrepancy ratio is classically employed in the
 234 literature (Van Rijn, 1984; Van den Berg, 1987; Batalla, 1997) and is defined as the ratio between the bedload rate
 235 estimated with the indirect method and the bedload rate using BTMA. Computed bedload layer volume
 236 concentration (Eq. 7) varies between 0.005 and 0.1 (0.03 in average). Bedload layer thickness (d_s) (Eq. 6) ranges
 237 between $1D_{50}$ and $7D_{50}$ ($5D_{50}$ in average). Bedload rates computed using Eq. (5) underestimate BTMA bedload
 238 rates with only 24% of the dataset in the discrepancy ratio (Figure 4b). By considering apparent bedload velocity
 239 without projection onto the flow direction, the kinematic model (Eq. 5) estimates satisfactorily BTMA bedload rates
 240 with 41% of the dataset in the discrepancy ratio. Conversely, using raw apparent bedload velocity in Eq. (4), leads
 241 to only 33% of the dataset in the discrepancy ratio against 54% with projected V_a . According to these results, Eq.
 242 (4) better describes the sampler bedload rates with projected apparent bedload velocity whereas raw apparent
 243 bedload velocity are preferred with Eq. (5). Some outlier data are observed for BTMA bedload discharge lower than
 244 $0.1 \text{ g.s}^{-1}.\text{m}^{-1}$. These points correspond to low flow conditions for which bedload samplers could under-estimate
 245 bedload fluxes (gap between the sampler mouth and the riverbed).



246

247 **Fig. 4: log/log correlation between bedload rates measured with BTMA sampler and calculated using a) Eq. (4) and; b)**
 248 **Eq. (5). Solid black line represents the perfect correlation and dashed black lines represents a factor of 2 above and**
 249 **below the perfect correlation.**

250 It appears difficult to estimate bedload rates only from dune celerity by assuming a direct relation between dune
 251 celerity and bedload transport rates measured with BTMA. Estimation of bedload transport rates from dune
 252 morphology has been performed by using empirical formula of Simons et al. (1965) (Eq. 13). The dataset is
 253 composed of 49 DTM profiles with associated BTMA samples. The mean dune height and length vary from 0.1 to
 254 0.5 m, and 1.3 to 12 m, respectively. The median dune celerity varies between 13 and 61 m.d⁻¹. According to Fig.
 255 4a, bedload rates estimated with a discharge coefficient $\beta = 0.33$ are in agreement with BTMA bedload rates with
 256 67% of values in a factor of 2 of the perfect correlation compared with 49% of values for a discharge coefficient of
 257 0.57 (Fig.5a). The definition of the discharge coefficient proposed by Engel and Lau (1980) is better adapted for
 258 the observed dune shapes found in the Loire River which are characterized by mean steepness (H_D/L_D)
 259 approximately equal to 0.05 (in line with other observations on the Loire River, Claude et al., 2012; Rodrigues et
 260 al., 2015; Wintenberger et al., 2015).



261

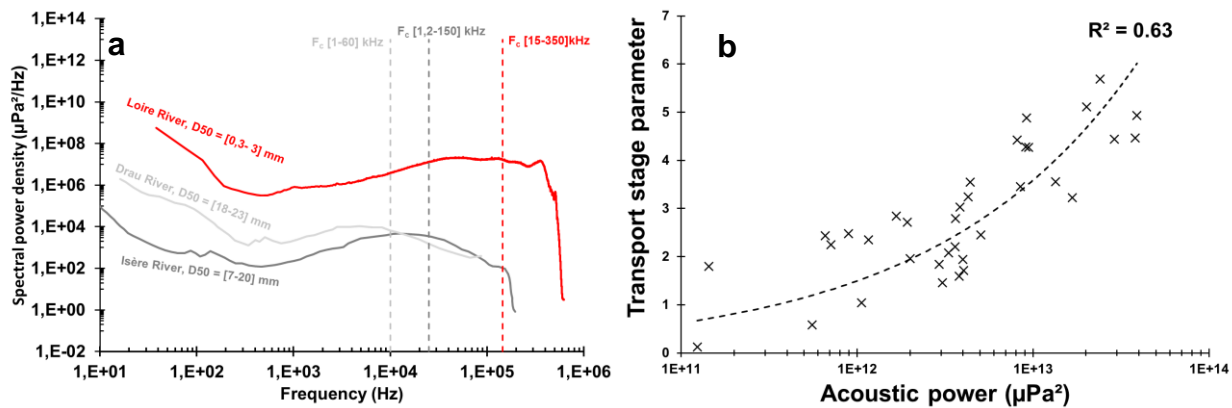
262 **Fig. 5: log/log correlation between bedload rates measured with BTMA samplers and bedload rates calculated using**
 263 **Eq. (13). Solid black line represents the perfect correlation and dashed black lines represents a factor 2 of the perfect**
 264 **correlation. b), unit bedload rates measured with BTMA samplers as a function of acoustic power measured with**

265 hydrophone. Dashed red lines represents the RMA regression with envelopes curves of a factor 2 of the bedload rates.
 266 Comparison with Geay et al. (2020).

267 Even if the statistical representativeness is lower than other methods (n=37), the RMA regression between the
 268 acoustic power and BTMA sampling is better ($R^2=0.70$) and 60% of values varying between a factor 2 (Fig. 5b). In
 269 consequence, new equation to estimate sediment transport from acoustic power is proposed:

$$270 P = 6.6 \times 10^{10} q_s^{1.32}; \quad (16)$$

271 This calibration curve is similar to observations performed by Geay et al. (2020) on 14 study sites distributed on 11
 272 different rivers despite the use of different instruments (sampler and hydrophone) and the integration of median
 273 PSD over a wider range of frequency in the present study. Moreover, the median PSD differ from the Isère River
 274 (Petruet et al., 2018) and from Drau River (Geay et al., 2017). These rivers are characterised by coarser sediments
 275 (see Fig. 6a) and the central frequency of the PSD are decreasing for an increasing D_{50} . These observations are
 276 in line with Thorne's (1986) theory. The central frequency of the median spectrum of the Loire River is approximately
 277 equal to 140 kHz. The frequency band of the bedload is shifted towards high frequencies due to finer grain size.
 278 The acoustic power corresponding to the integration of the spectrum over a range of frequency is related to the
 279 grain size (Thorne, 1985) and sediment kinematics (Gimbert et al., 2019). To analyse the effect of sediment mobility
 280 on the acoustic power, the transport stage parameter (Van Rijn, 1984) is calculated. The power law adjusted
 281 between these two parameters evidences a positive evolution of the acoustic power with sediment mobility (Fig.
 282 6b).



283
 284 **Fig. 6: (a), Comparison of PSD from 3 rivers with varying D_{50} . (b), transport stage parameter (from Van Rijn, 1984) as a**
 285 **function of acoustic power.**

286 The comparison can be performed between indirect methods to discuss the acceptability of the BTMA reference.
 287 The apparent bedload velocity and the acoustic power are poorly correlated with mean dune morphological
 288 parameters (Table 1).

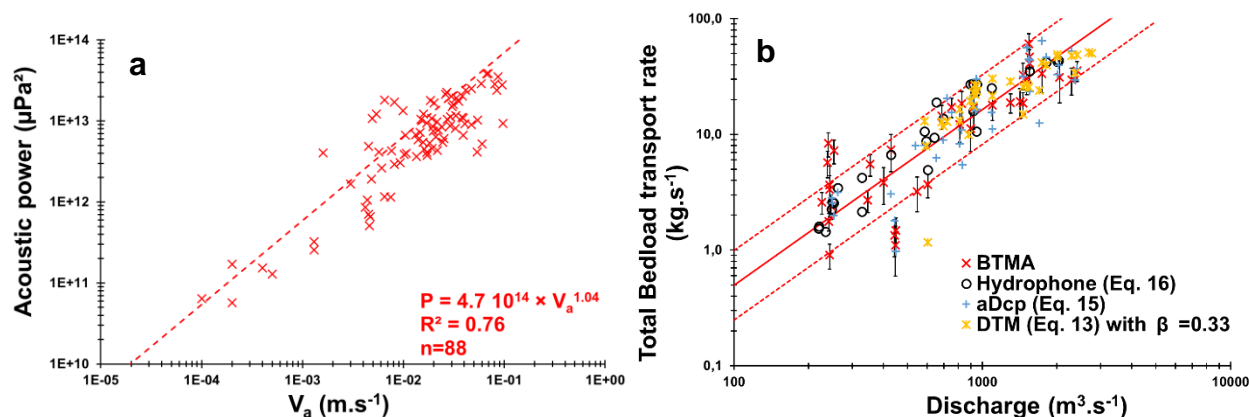
289 **Table 1: Coefficient of determination (COD) between dune parameters and acoustic methods (log values).**

	P	V _a	Q _s BTMA	H _{dune}	C _{dune}
H _{dune}	0.20	0.27	0.16	-	-
C _{dune}	0.22	0.24	0.36	0.22	-

290

291 The apparent velocity measures the top layer velocity or dynamical active layer (sediment being transported over
 292 a dune), whereas the dune celerity is the mobility of the exchange event active layer, according to Church and
 293 Haschenburger (2017). It must be noted that apparent bedload velocity is higher than dune celerity by a factor
 294 approximately equal to 100. On the other hand, the apparent bedload velocity is positively correlated with the
 295 acoustic power. The COD of the RMA regression is equal to 0.76 (Fig. 7a).

296 Before focusing on the spatial distribution of unit bedload rates, total bedload rates are calculated by interpolating
 297 unit bedload rates between sampling points on the cross section for each method. The COD of the RMA regression
 298 established between BTMA bedload rates and water discharge is 0.71 (Fig. 7b) with 77% of the values varying in
 299 a factor 2. The dispersion of bedload rates is higher for low water discharge (under mean annual discharge, 800
 300 m³.s⁻¹). Bedload rates are estimated from Eqs. (13), (15) and (16), for the DTM, the aDcp and the hydrophone,
 301 respectively. Both the hydrophone and DTM bedload rates are less scattered with 96% of values in the discrepancy
 302 ratio, compared with 82% for the aDcp.



303

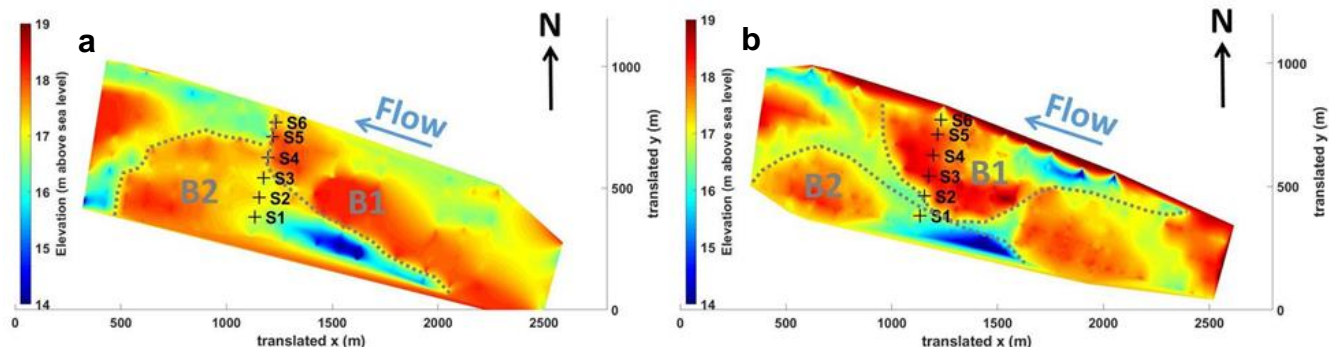
304 **Fig. 7: (a), acoustic power as a function of apparent bedload velocity. (b), Cross section integrated bedload transport**
 305 **rates as a function of discharge.**

306 4.2. Spatial distribution of bedload in a sandy gravel-bed river with migrating bedforms

307 4.2.1. Determination of bedload transport on a cross section using acoustics methods

308 To compare the spatio-temporal distribution of bedload transport rates, sediment transport sampling was performed
 309 on the same cross section for all surveys and for various discharge conditions. Two surveys with contrasting
 310 discharge conditions and different bed configurations are presented (Fig. 8) to illustrate the capability of acoustics

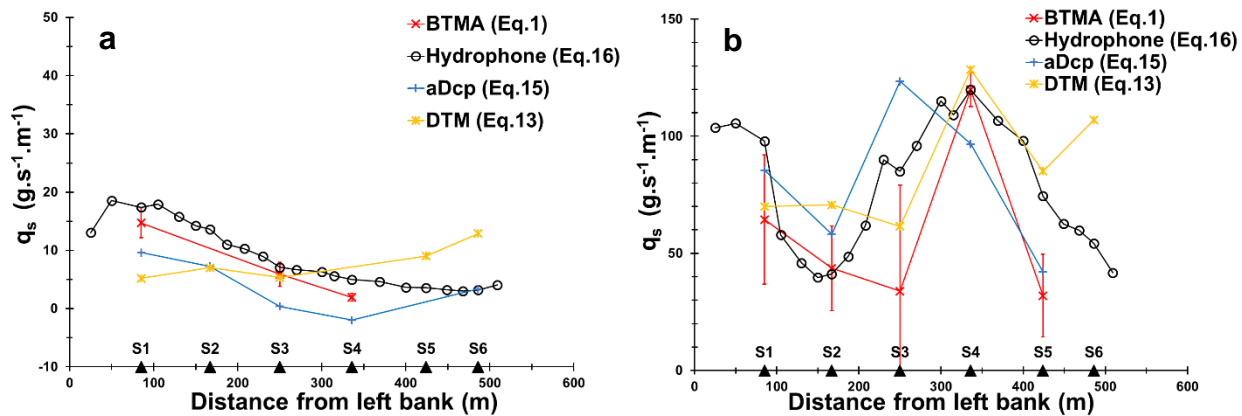
311 methods to determine bedload active width in a river reach characterized by the presence of macroforms and
312 superimposed mesoforms (*sensu lato*, Jackson, 1975).



313

314 **Fig. 8: Bathymetric Digital Elevation Models (obtained using natural neighbours interpolation) showing location of**
315 **sampling points with respect to bar location during: (a), survey of the 17/05/2018 ($Q=604 \text{ m}^3 \cdot \text{s}^{-1}$) and (b), survey of the**
316 **19/12/2019 ($Q=2050 \text{ m}^3 \cdot \text{s}^{-1}$).**

317 In May 2018, a bar (B1, Fig. 8a) was located just upstream the sediment gauging section from the center to the
318 right part of the channel. In the left part of the channel, BTMA sampling was performed on the stoss side of another
319 bar (B2, Fig. 8a). Consequently, bedload rates gradually rose from the center of the channel ($2 \text{ g} \cdot \text{s}^{-1} \cdot \text{m}^{-1}$, S4) to the
320 left part of the channel ($15 \text{ g} \cdot \text{s}^{-1} \cdot \text{m}^{-1}$, S1) except for the DTM (Fig. 9a). The intensity of bedload transport rates was
321 evaluated for each acoustic signal from regression equations established above (Eqs. 13, 15 and 16, for DTM,
322 aDcp and hydrophone, respectively). The linear equation of aDcp calibration allow the calculation of negatives
323 bedload flux for apparent bedload velocity below $0.0016 \text{ m} \cdot \text{s}^{-1}$ (Fig. 9a, S4). ADcp and hydrophone signals followed
324 the same trend as the BTMA measurement. In the right part of the channel, no reference measurements were
325 available (S5 and S6) but all acoustic signals followed the same trend (increasing bedload transport rates). The
326 bedload rates estimated with the DTM were lower than the reference in the left part of the channel. This can be
327 explained by the reduced number of dunes in this area that caused a higher uncertainty in dune celerity
328 determination. In the right part, the proximity of the bar front induced lower bedload transport rates measured with
329 aDcp and hydrophone. DTM integrates sediment dynamics over a longitudinal profile that does not necessarily
330 reflect the bedload transport conditions at a local scale. Due to the lee effect provided by the proximity of the bar
331 front, dunes were not present downstream of the bar and only dunes located on the stoss side of the bar were used
332 to calculate the mean dune celerity. ADcp underestimates whereas the hydrophone method overestimates the unit
333 bedload rate compared with BTMA measurements.



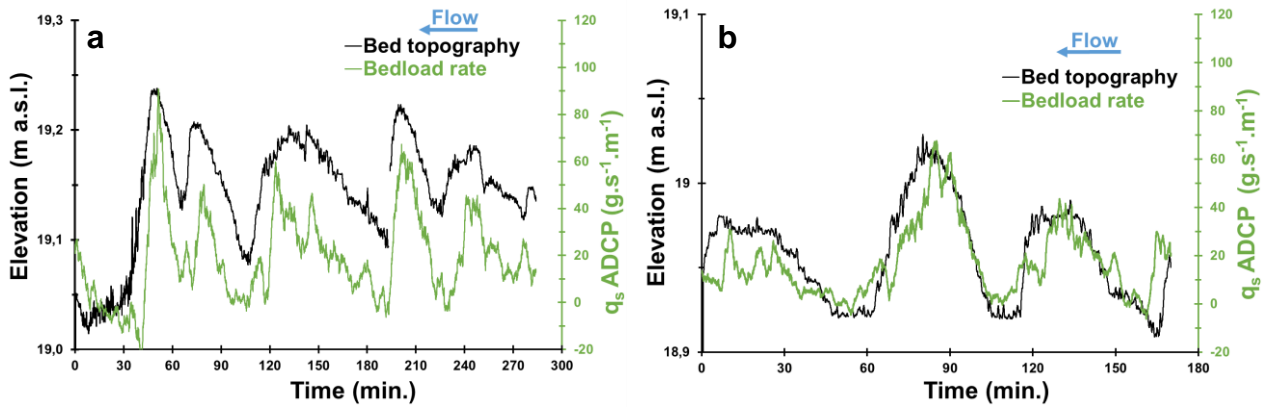
334

335 **Fig. 9: Lateral distribution of unit bedload rates assessed from different methods for two surveys performed: (a), the**
 336 **17/05/2018 ($Q=604 \text{ m}^3 \cdot \text{s}^{-1}$) and (b), the 19/12/2019 ($Q=2050 \text{ m}^3 \cdot \text{s}^{-1}$), respectively.**

337 In December 2019 (Fig. 9b), the flow discharge was higher ($2050 \text{ m}^3 \cdot \text{s}^{-1}$) than the value observed in May 2018
 338 ($Q=604 \text{ m}^3 \cdot \text{s}^{-1}$) and measured bedload rates ranged between 32 and $120 \text{ g} \cdot \text{s}^{-1} \cdot \text{m}^{-1}$. Due to the bar migration, the
 339 bed configuration was different. Bar B1 reached the sediment gauging cross section. As a consequence, sampling
 340 points S3 to S6 were located on the stoss side of bar B1 (Fig. 8b). The sampling point S2 was located just
 341 downstream the bar front where the velocity and sediment transport rates were lower (Fig. 8b). The high spatial
 342 resolution of the hydrophone measurements confirmed that the preferential bedload active width was located
 343 between 250 and 450 m from the left bank (Fig. 9b). For this survey, acoustic signals (*i.e.* acoustic power, apparent
 344 bedload velocity) followed the same evolution pattern as samplers along the cross section except for S3. Bedload
 345 transport rates determined with the DTM did not follow the trend of bedload rates determined with aDcp and
 346 hydrophone at the proximity of bar front and near the bank as in the previous survey (S2 and S6). The hydrophone
 347 model overestimated the sediment transport in comparison with the BTMAs for S1, S3 and S5.

348 4.2.2. Sediment transport processes on bedforms analyzed from aDcp and hydrophone

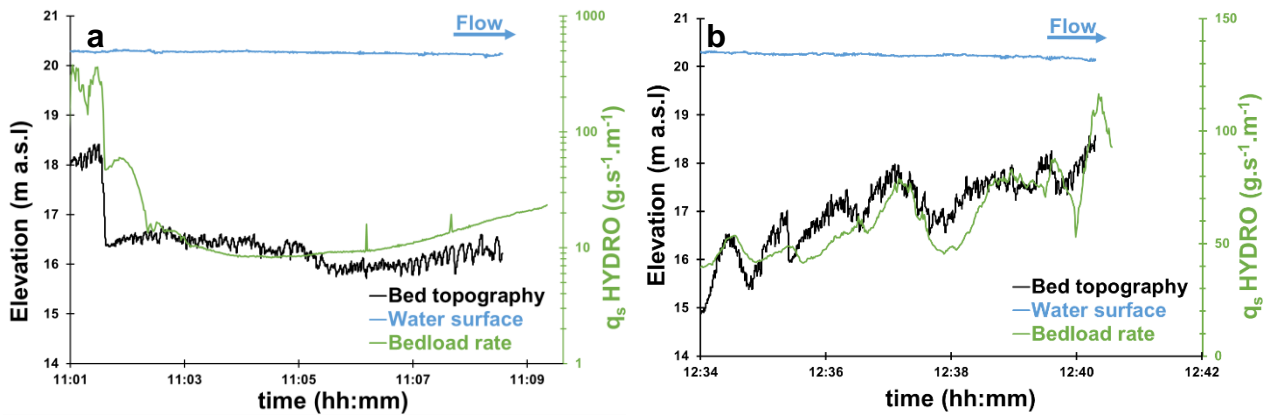
349 The aDcp computed bedload rates evolved according to bedform location for fixed measurements performed on
 350 dunes of height ranging between 0.05 m and 0.2 m (Fig. 10a and 10b). Higher bedload rates values were found on
 351 the crest of the dune and lower values in the trough. The amplitude of bedload rates between crest and trough for
 352 low flow conditions (Fig. 10b) ranged between $42 \text{ g} \cdot \text{s}^{-1} \cdot \text{m}^{-1}$ and $67 \text{ g} \cdot \text{s}^{-1} \cdot \text{m}^{-1}$. For higher flow conditions, it varied
 353 between $45 \text{ g} \cdot \text{s}^{-1} \cdot \text{m}^{-1}$ and $91 \text{ g} \cdot \text{s}^{-1} \cdot \text{m}^{-1}$ (Fig. 10a). These values were extracted considering bedload rates in trough
 354 as equal to zero (not negative). The aDcp linear regression (Eq. 15) did not allow the calculation of bedload
 355 transport rates due to negative apparent bedload velocity. This is the case downstream the lee face of dunes (Fig.
 356 10a, between 8 to 42 min., 96 to 107 min., 185 to 193 min., and 227 to 230 min.; Fig. 10b, between 48 to 55 min.
 357 and 153 to 162 min.). The mean time recorded between two successive dune crests was 1 hour.



358

359 **Fig. 10: Bedload rates calculated using Eq. (15) and bed topography obtained during a static measurement performed**
 360 **using an aDcp. (a), survey done the 20/05/2020 ($Q=470 \text{ m}^3\cdot\text{s}^{-1}$; mean water depth = 1.04 m) and (b), survey done the**
 361 **29/05/2019 ($Q=210 \text{ m}^3\cdot\text{s}^{-1}$; mean water depth = 0.85 m).**

362 Hydrophone drifts showed that the longitudinal evolution of acoustic power can be correlated with changes in
 363 elevation of the riverbed due to dune and bar presence. For instance, in the presence of a 2 meter high bar front,
 364 the bedload rate significantly decreased, illustrating the lee effect that is characterised by a decrease in bedload
 365 sediment transport (Fig. 11a). This shows that the hydrophone is sensitive enough to detect this local phenomenon
 366 induced by the presence of a bar front immediately upstream. The bedload rates range from about $8 \text{ g}\cdot\text{s}^{-1}\cdot\text{m}^{-1}$ on
 367 the bar crest to $376 \text{ g}\cdot\text{s}^{-1}\cdot\text{m}^{-1}$ in the bar trough ($1 \cdot 10^{12} \text{ }\mu\text{Pa}^2$ to $1.7 \cdot 10^{14} \text{ }\mu\text{Pa}^2$ of acoustic power, respectively).
 368 According to flow velocity measurements, it appears that a 2 m high bar front can influence flow velocity and
 369 bedload transport rates up to the reattachment point located approximately 100 m downstream. Downstream the
 370 bar front, the bedload transport rate increased from 11h06min (Fig. 11a) that would be in coincidence with the flow
 371 reattachment point. Further downstream, the bedload transport rate increased from 8.5 to $23.4 \text{ g}\cdot\text{s}^{-1}\cdot\text{m}^{-1}$
 372 (representing respectively an acoustic power of $1.2 \times 10^{12} \text{ }\mu\text{Pa}^2$ to $4.1 \times 10^{12} \text{ }\mu\text{Pa}^2$), where dunes exhibit a more
 373 regular shape increasing their amplitudes from 0.02 m to 0.4 m, approximately. On the left part of the channel (Fig.
 374 11b), the drift was located at the stoss side of a bar where larger dunes were observed (about 1 m in height) with
 375 superimposed small dunes (height approximately equal to 0.3 m). The bedload transport rate calculated above
 376 these bedforms increased near the crests of the large dunes (about $80 \text{ g}\cdot\text{s}^{-1}\cdot\text{m}^{-1}$) and decreased in the troughs
 377 (about $50 \text{ g}\cdot\text{s}^{-1}\cdot\text{m}^{-1}$) where superimposed bedforms were smaller (Fig. 11b).



378

379 **Fig. 11: Bedload rates calculated on bedforms using the hydrophone and Eq. (16) near a bar front (a) and on a dune**
 380 **field (b). Bed topography and water surface along two longitudinal bathymetric profiles for the 08/02/2018 survey,**
 381 **$Q=1550 \text{ m}^3\cdot\text{s}^{-1}$: (a), P10, mean water depth = 3.8 m. The profile length from 11:01 to 11:09 corresponds to 400 m; (b),**
 382 **P12, mean water depth = 3.4 m. The profile length from 12:34 to 12:41 corresponds to 518 m.**

383 5. Discussion

384 5.1. Relevance of acoustics for computing bedload transport rates

385 Despite their lack of accuracy and their low spatial representativeness, samplers allow a direct measurement of
 386 bedload and represents the only reference measurement of bedload in the field. The presence of bars affect
 387 sediment transport locally and make sampling method very sensitive to the location of the sampling point. For low
 388 water discharge (below mean annual discharge, $800 \text{ m}^3\cdot\text{s}^{-1}$), bars are emerged and reduce considerably the width
 389 where sediment transport occurs. The number of sampling points decrease with discharge (because bars were not
 390 flooded) leading to a higher bedload rates variability (Fig. 7b). Moreover, in weak bedload transport conditions, the
 391 BTMA sampler most likely performed with reduced efficiency initially calibrated to 50%, (van Rijn and Gaweesh,
 392 1992; Gaweesh and van Rijn, 1994; Banhold et al., 2016). The presence of dunes influences the performance of
 393 the sampler by preventing the exact positioning of sampler mouth on the river bed. These deficiencies lead to a
 394 large uncertainty in bedload estimation which set the limits of the comparison with other methods.

395 The use of hydrophones to estimate bedload transport in a lowland sandy gravel-bed river constitutes a new
 396 research topic. As discussed by several authors, the use of hydrophones was so far restrained to gravel-bed rivers
 397 (Bedeus and Ivicsics, 1963; Barton et al., 2010; Hilldale et al., 2014; Thorne, 2014; Marineau et al., 2016; Geay et
 398 al., 2017) or marine environments (Thorne et al., 1984; Thorne, 1986; Blanpain et al., 2015). More recently, Geay
 399 et al. (2020) highlighted that the acoustic power measured with a hydrophone can be correlated to the sampler
 400 measurements of bedload in fluvial environments characterized by bed slopes varying between 0.05 and 2.5% and
 401 channel width ranging between 8 and 60 m. In these mountainous environments, the median grain size ranged
 402 between 0.9 and 62 mm ($n=582$ samples). In our study, the downstream reach of the Loire River shows smaller

403 slope ($S=0.02\%$), a wider channel ($W=500$ m), and a median grain size ranging between 0.3 mm to 3.1 mm ($n=450$
404 samples). The hydrophone is therefore an efficient tool for sediment transport gauging, allowing the measurement
405 of numerous sampling points (average of 17 sampling points) during a relatively shorter time period (one hour).
406 This high spatial discretization makes the hydrophone functional over a wide range of discharges (even for low
407 water discharge, Fig. 6b) by catching the high spatial variability of bedload transport. It should be pointed that the
408 regression calculated in the present study (Eq. 16) is obtained from unit bedload rates (from several samples) and
409 the acoustic power resulting to a unique acoustical drift, whereas Geay et al. (2020) compared averaged cross
410 section bedload rates and acoustic power. Despite these differences, the data presented above corroborate the
411 results by Geay et al. (2020) and support their conclusions concerning the determination of a global calibration
412 curve between acoustic power and bedload rates by extending its application to the lowland sandy gravel-bed
413 rivers. Although this need to be confirmed by further investigations to better understand parameters that control the
414 acoustic power measured (such as the propagation of sound waves in water (Geay et al., 2019) and their
415 attenuation, the saltation length and associated impact celerity, or sediment grain size), results presented in this
416 study suggest that the hydrophone method could be an efficient way to measure and to map bedload transport
417 rates on a wider range of fluvial systems.

418 Several laboratory studies have been carried out (Ramooz and Rennie, 2010; Conevski et al., 2019; Conevski et
419 al., 2020b) and rivers instrumented with aDcp to determine bedload rates (Rennie et al., 2002; Rennie and Millar,
420 2004; Gaeuman and Jacobson, 2006; Gaeuman and Pittman, 2010; Brasington et al., 2011; Conevski et al.,
421 2020a). Recent works have been carried out on two rivers (Elbe, Oder) similar to the Loire River in term of grain
422 size characteristics, flow and shear velocity, and water depth (Conevski et al., 2020a). Even if the correlation
423 between apparent bedload velocity and bedload rates is significant, this calibration equation was obtained from two
424 very similar rivers. Despite these observations, there is no general agreement between bedload rates and apparent
425 velocity (Rennie and Villard, 2004; Rennie et al., 2017). The response of aDcp to bedload transport depends on
426 several parameters The variation of the impulse frequency, the pulse length, beam focusing or associated internal
427 signal processing (Broadband or Narrowband) can lead to different estimation of the apparent bedload velocity for
428 the same sediment transport conditions (Conevski et al., 2020a). These parameters vary from a device to another
429 (RDI/Sontek; Conevski et al., 2020b). As the aDcp pulse sample a volume of the riverbed (Rennie et al., 2002)
430 which can lead to a biased estimation of V_a : *i*) an underestimation in case of large roughness of the riverbed with
431 most of the reflected pulse is scattered by the immobile particles below the active layer (Conevski et al., 2019); *ii*)
432 an overestimation in case of high concentration of the bedload layer (Rennie et al., 2017) or sand particles became
433 in suspension near to the riverbed (water bias, Rennie et Millar, 2004). Even if a general trend seems to be
434 highlighted by the river comparison (figure 3a) with an increasing bedload rate as grain size increases for a constant
435 V_a , the relationship between grain size and V_a cannot be easily determined in response to all variables mentioned
436 above. One explanation of this trend could be that suspended sands could contribute to the bottom tracking signal

437 without being caught by the sampler (Rennie et al., 2017). Moreover, the accuracy of the measurement on a single
438 cross section depends on the water depth heterogeneity that in turn influences the aDcp footprint and makes the
439 aDcp method location sensitive when bedforms are present (Fig. 9b). Estimation of bedload rates using empirical
440 equations is limited by the number of variables that are difficult to measure in the field (e.g. thickness and
441 concentration of active layer, Kostaschuck et al., 2005; Villard et al., 2005; Holmes, 2010; Latosinski et al., 2017;
442 Conevski et al., 2018). The results shown in Fig. 4a suggest that Eq. (4) estimates sampler bedload rates if the
443 projected bedload velocity is used. This kinematic model does not account for the thickness or the sediment
444 concentration of the bedload layer and assumes that bedload transport never exceeds the size of a single particle
445 assessed as uniform in terms of grain size (Rennie et al., 2002). These assumptions seems not appropriated for a
446 sandy-gravel bed river. The active layer thickness should increase as suspended bed material load increases.
447 Nevertheless, results are in agreement with BTMA bedload rates (Figure 4a). This can be explained by an
448 underestimation of the apparent bedload velocity when it is projected along flow direction. On the other hand, Van
449 Rijn (1984) defined the bedload layer thickness equal to the saltation height. The computed values of bedload layer
450 thickness are coherent with other estimations performed on comparable rivers (Conevski et al., 2020a). The Eq.
451 (5) better estimates sampler bedload rates using the raw bedload velocity (Figure 4b). If we consider that c_b and d_s
452 are well estimated by van Rijn equations (Eqs. 6 and 7), these results confirm that the projection of the apparent
453 bedload velocity decreases the bedload velocity magnitude when the bedload direction differs from flow direction
454 (e.g. bed slope effects). The influence of bedload velocity projection appears to be important when bedload are
455 computed using kinematic models. Nevertheless, the calibration curve seems to be in agreement with other studies.
456 Although, the application domain of Eq. (4) does not correspond to the conditions in the Loire River, the decrease
457 of projected V_a seems to compensate the overestimation of bedload rates when the raw apparent bedload velocity
458 is used. This is the opposite for Eq. (5) that accounts for bedload layer thickness and sediment concentration. In
459 this case, the projection of V_a leads to underestimate bedload rates. Further works need to be done to improve the
460 post-processing of V_a by recently published filtering procedures (Conevski et al., 2019 and 2020a) and to estimate
461 its effect on calibration curve and kinematic models.

462 Contrarily to the aDcp, the DTM allows the investigation of the “event active layer” (Church and Haschenburger,
463 2017). The DTM is not a punctual measurement of bedload. Consequently, in presence of macroforms such as
464 bars, it is difficult to compare with BTMA samples because it takes into account dunes that are not necessarily
465 present at the BTMA sampling point (typically downstream a bar lee side). To some extent, the DTM and BTMA
466 methods integrate bedload longitudinally at different scales. The presence of a local disturbance (or migrating
467 bedform at low celerity) will affect the measurement. The determination of dune celerity by post-processing is time-
468 consuming compared with the determination of dune morphology and the existing open access post-processing
469 tools. In order to determine bedload rates with empirical equations, this method needs a calibration coefficient that
470 is difficult to measure in field studies (Ten Brinke et al., 1999; Wilbers, 2004). Moreover, physical samplers sample

471 the dynamical active layer, thus more comparable to the hydrophones and aDcps. Nevertheless, DTM remains an
472 accurate method to estimate bedload transport in the Loire River (Fig. 6b) where dunes are present and high
473 enough (over the mean annual discharge).

474 As suggested by previous authors, both aDcp (Kenney, 2006) and hydrophone (Bedeus and Ivicsics, 1963) allow
475 a reliable representation of bedload fluxes on a cross section through the regressions with bedload rates obtained
476 using samplers. Fig. 9a and Fig. 9b highlight the benefits of the use of acoustics devices for the determination of
477 bedload transport rates in a large sandy gravel-bed rivers. In the present study, the time needed in the field to
478 complete the BTMA, DTM, aDcp and hydrophone methods (respectively the red, yellow, blue and black lines of
479 Fig. 9b) are about 1 day, 4 hours, 1.5 hours and 45 minutes, respectively. These times were estimated including
480 the time needed to position and anchor the boat at each sampling point. This underlines the high potential of
481 hydrophones to quantify bedload in large rivers with high spatial variability of sediment transport and map bedload
482 sediment fluxes at a large scale as proposed by Williams et al. (2015) using the aDcp. Moreover, all indirect
483 methods tested here seem to be able to quantify total bedload transport as efficient as the direct method (Fig. 6b)
484 but special care should be taken with local estimation of bedload rates (Fig. 9a and Fig. 9b).

485 Finally, regarding the correlation of aDcp and hydrophone with BTMA (Fig. 3a and Fig. 5b), we can raise the
486 question of the reference method. Indeed, the regression between aDcp and hydrophone is more significant
487 ($R^2=0.76$) and it could be the quality and the accuracy of BTMA sampling that reduce the quality of indirect
488 measurement regressions.

489 **5.2. Hydrophone and aDcp sensitivity to bedform observations**

490 Passive (hydrophone) and active (aDcp) acoustic devices are rarely used to analyse of bedload transport rates
491 associated with bedforms in relatively large lowland rivers. Several studies mention differences in apparent bedload
492 velocity according to the location on bedforms (Rennie and Millar, 2004; Villard and Church, 2005; Gaeuman and
493 Jacobson, 2006; Holmes, 2010; Latosinski et al., 2017). These authors have shown that apparent bedload velocity
494 increases from trough to crest of the dune and confirmed previous observations made with samplers (Kostachuck
495 and Villard, 1996; Carling et al., 2000). These observations were made on large dunes that migrate too slowly to
496 allow a continuous measurement along bedforms. Our study complements these observations by providing a fixed
497 and continuous measurement of apparent bedload velocity and providing bedload transport rates estimation based
498 on a calibration curve. The mean time between two subsequent crests (1 hour) shows that even for small bedforms
499 ($H_D = 0.05$ to 0.2 m, Fig. 10a and Fig. 10b), the aDcp location significantly influences the bedload rates calculated
500 over a dune field (0.03 to 0.08 $\text{m}\cdot\text{s}^{-1}$ of difference between crest and trough). This suggests that care should be
501 taken using this method on river beds where large dunes are present but also when small dunes are migrating.
502 According to Rennie and Millar (2004), the sampling area diameter increases with the water depth and is
503 approximately equal to flow depth. Our protocol minimizes the water depth by submerging the aDcp and therefore

504 minimizes the beams sampling diameter, hence, minimizes the probability to sample stoss or lee sides of the same
505 dune simultaneously.

506 In our study context, the acoustic power recorded by the hydrophone was not affected by the distance between the
507 hydrophone and the river bed. To our knowledge, there are no references mentioning investigations on bedload
508 transport rates associated with bedforms using a hydrophone. At a large time step (mean aDcp and hydrophone
509 samples), the apparent bedload velocity and the acoustic power did not follow the observed trend of mean bedform
510 characteristics derived from DTM measurement (dune celerity and dune height). This could be explained by the
511 difference of spatial scales between DTM and other methods. For a smaller time step, our results showed that
512 acoustic power is able to describe the influence of bars on bedload sediment transport (Fig. 11a). Moreover, as for
513 the aDcp, the hydrophone also detects the theoretical pattern of bedload transport rates associated with bedform
514 migration. As shown by Reesink et al. (2014), the lee effect generated by bar fronts influences the development of
515 dunes downstream. Specifically, the hydrophone is able to record the decrease of the acoustic power immediately
516 downstream the bar front and its progressive increase downstream (traduced by the development of dunes at about
517 11h06, Fig. 11a). In the present study, dunes smaller than 0.4 m (Fig. 11a) were not high enough to allow the
518 observation of changes in the acoustic power along the bedform stoss sides. On the contrary, for higher dunes (H_D
519 = 1 m, Fig. 11b) the bedload generated noise can be well recorded by the hydrophone. A hydrophone senses every
520 noises that are propagating in the water column. Therefore, the hydrophone can record noises that is far away from
521 its location. Noises are more and more attenuated with increasing distance (Geay et al., 2019). Particularly, when
522 there is few bedload noise close to the hydrophone, the hydrophone can sense the bedload noise that are
523 generated far away. This behaviour could explain why the hydrophone tends to overestimate bedload fluxes when
524 bedload fluxes are weak especially immediately downstream a bar front (Fig. 9b).

525 Hydrophone lower detection limit was not reached during our study whereas the dispersion of bedload rates
526 measured with samplers for low apparent bedload velocity suggests that the lower detection limit of the apparent
527 bedload velocity by the aDcp seems to be about 1 cm.s^{-1} (Rennie et al., 2017). This lower detection limit of the
528 apparent bedload velocity should be reduced to the bottom track uncertainty by using our protocol with a
529 submerged and fixed aDcp device.

530 **6. Conclusions**

531 In this work, direct (BTMA samplers) with active (aDcp and DTM) and passive (hydrophone) acoustic
532 measurements of bedload transport rates were compared in a large, sandy-gravel bed river characterized by the
533 presence of bars and superimposed dunes. Calibration curves between apparent bedload velocity measured using
534 aDcp and bedload rates measured using BTMA samplers were established but remain site-specific and dependent
535 to grain size. DTM seemed to be inappropriate where macroforms are present, as it influences the location and the

536 size of superimposed mesoforms. The calculation of bedload rates with empirical formulas is sensitive to bedload
537 discharge coefficient for DTM and to thickness and concentration of active layer for aDcp. These parameters remain
538 difficult to measure in the field. Results presented in this study highlight the potential of the hydrophone for the
539 quantification and mapping of bedload transport rates in relatively large river channels where migrating bedforms
540 are present while it was mainly used until today to monitor bedload transport rates in gravel-bed rivers. This study
541 consolidates a recent study (Geay et al., 2020) by extending a general calibration curve to large sandy-gravel bed
542 rivers. The hydrophone global calibration curve allows a good representation of the bedload fluxes evolution
543 through a cross section. The method is more affordable to implement and more efficient than the reference method.
544 This might allow mapping bedload transport rates by interpolating acoustic power along several cross sections
545 performed on a large sandy gravel bed river. Moreover, acoustic devices (aDcp and hydrophone) are able to
546 capture the evolution of bedload signal along bedforms stoss and lee sides with some limitation of bedform size for
547 the hydrophone and signal noise for the aDcp. Regarding results of the comparison between bedload velocity and
548 acoustic power, the association of aDcp and hydrophone could be an efficient way to control the quality of both
549 devices. However, additional measurements and post-processing tasks are needed (Conevski et al., 2019) to
550 explore the quality of the regression in other river environments (different grain sizes, river-bed slope or propagation
551 effect).
552

553 **Appendices**

554 Appendix A: Hydrophone dataset

555

Date	Number of Hydrophone Drifts	average drift duration (s)	mean acoustic power (Pa ²)
08/02/2018	24	60	2.17E+13
17/05/2018	24	80	1.46E+12
15/04/2019	11	37	1.66E+12
16/04/2019	11	42	2.25E+12
17/04/2019	11	28	1.42E+12
18/04/2019	11	30	2.35E+12
27/05/2019	8	42	5.07E+11
29/05/2019	9	36	2.00E+12
09/12/2019	22	29	6.67E+12
10/12/2019	21	22	7.69E+12
11/12/2019	22	27	8.84E+12
12/12/2019	13	27	8.97E+12
19/12/2019	22	25	2.41E+13
18/05/2020	8	50	4.53E+12
19/05/2020	8	30	3.82E+12
20/05/2020	17	36	3.07E+12

556

557

Date	Number of aDcp sampling points	aDcp frequency (kHz)	aDcp type *1	Pulse type *2	Average aDcp sampling duration (s)	mean Va (m.s ⁻¹)	mean water depth (m)	mean flow velocity (m.s ⁻¹)
27/03/2017	4	1200	RG	BB	3909	0.013	2.0	0.7
28/03/2017	4	1200	RG	BB	3279	0.015	2.1	0.7
29/03/2017	4	1200	RG	BB	3276	0.011	2.2	0.7
30/03/2017	4	1200	RG	BB	1707	0.009	2.1	0.8
15/05/2017	3	1200	RG	BB	3018	0.002	1.3	0.8
16/05/2017	2	1200	RG	BB	2315	0.010	1.0	0.8
17/05/2017	3	1200	RG	BB	2618	0.003	1.4	0.8
18/05/2017	3	1200	RG	BB	2467	0.002	1.6	0.8
04/12/2017	3	1200	RG	BB	2647	0.000	1.2	0.7
05/12/2017	3	1200	RG	BB	2657	0.008	1.2	0.6
06/12/2017	3	1200	RG	BB	2246	0.000	1.2	0.7
07/12/2017	3	1200	RG	BB	2588	0.002	1.3	0.7
08/12/2017	3	1200	RG	BB	3400	0.003	1.2	0.6
15/01/2018	3	1200	RG	BB	3256	0.084	3.2	1.1
16/01/2018	3	1200	RG	BB	1800	0.058	2.9	1.0
17/01/2018	4	1200	RG	BB	3185	0.041	2.7	1.0
18/01/2018	4	1200	RG	BB	3656	0.055	2.8	1.0
19/01/2018	3	1200	RG	BB	2029	0.075	2.7	1.1
30/01/2018	3	1200	RG	BB	2138	0.051	3.9	1.1
31/01/2018	3	1200	RG	BB	2056	0.070	3.7	1.1
08/02/2018	4	3000	M9	BB	1136	0.038	2.8	0.9
14/05/2018	4	3000	M9	BB	2130	0.002	1.2	0.6
15/05/2018	4	variable	M9	HD	1133	0.011	1.5	0.6
16/05/2018	3	variable	M9	HD	948	0.002	1.4	0.7
17/05/2018	3	1200	RG	BB	1346	0.003	1.7	0.7
15/04/2019	3	variable	M9	HD	2601	0.009	1.2	0.8
16/04/2019	3	3000	M9	NB	1687	0.006	1.1	0.7
17/04/2019	3	variable	M9	HD	1152	0.010	1.0	0.7
18/04/2019	3	variable	M9	HD	3580	0.008	0.9	0.7

27/05/2019	1	3000	M9	NB	10949	0.003	0.9	0.8
29/05/2019	1	3000	M9	NB	11539	0.029	0.9	0.7
09/12/2019	2	3000	M9	NB	1753	0.023	1.7	0.8
10/12/2019	3	3000	M9	NB	1160	0.018	2.1	0.8
11/12/2019	3	3000	M9	NB	1288	0.027	1.6	0.9
12/12/2019	2	3000	M9	NB	1349	0.032	2.1	0.8
19/12/2019	5	3000	M9	NB	1221	0.056	3.0	1.1
19/05/2020	2	3000	M9	NB	7318	0.014	1.0	0.7
20/05/2020	4	3000	M9	NB	2988	0.004	1.6	0.7

560 *1: RG = aDcp Rio Grande RDI; M9 = aDcp M9 Sontek

561 *2 BB = Broadband (coherent Pulse); NB = Narrowband (incoherent pulse); HD = Smartpulse HD

562

Date	Discharge (m ³ .s ⁻¹)	Measurements type	Number of BTMA sampling points	Number of BTMA samples	Mean unit bedload rate (g.s ⁻¹ .m ⁻¹)	D50 (mm)	D90 (mm)
28/11/2016	1420	BTMA & DTM	3	50	38.1	0.8	3.0
29/11/2016	1460	BTMA & DTM	4	79	31.5	0.9	3.5
30/11/2016	1300	BTMA & DTM	4	80	33.2	0.8	2.9
01/12/2016	1100	BTMA & DTM	4	79	32.2	0.8	2.6
27/03/2017	687	BTMA. aDcp & DTM	4	80	25.3	0.7	2.9
28/03/2017	752	BTMA. aDcp & DTM	4	80	28.5	0.8	3.0
29/03/2017	827	BTMA. aDcp & DTM	4	57	29.0	0.8	3.8
30/03/2017	812	BTMA. aDcp & DTM	4	80	19.3	0.8	3.8
15/05/2017	346	BTMA. aDcp & DTM	3	60	6.3	0.9	4.8
16/05/2017	354	BTMA. aDcp & DTM	3	60	13.5	0.8	5.0
17/05/2017	401	BTMA. aDcp & DTM	3	55	9.0	0.9	4.7
18/05/2017	447	BTMA. aDcp & DTM	3	60	1.9	1.2	7.0
04/12/2017	243	BTMA & aDcp	3	60	1.8	1.1	7.4
05/12/2017	241	BTMA. aDcp & DTM	3	60	3.7	1.0	8.6
06/12/2017	243	BTMA. aDcp & DTM	3	60	6.6	1.2	6.7
07/12/2017	246	BTMA. aDcp & DTM	3	60	5.1	1.2	5.1
08/12/2017	226	BTMA. aDcp & DTM	3	60	5.0	1.6	7.9
15/01/2018	1740	BTMA. aDcp & DTM	3	60	61.4	1.0	2.9
16/01/2018	1550	BTMA. aDcp & DTM	3	60	89.4	0.9	2.8
17/01/2018	1460	BTMA. aDcp & DTM	4	80	53.2	0.8	3.0
18/01/2018	1540	BTMA. aDcp & DTM	4	80	97.7	1.0	3.3
19/01/2018	1510	BTMA. aDcp & DTM	3	60	55.6	0.8	2.6
30/01/2018	2410	BTMA. aDcp & DTM	3	60	68.6	0.8	2.3
31/01/2018	2290	BTMA. aDcp & DTM	3	59	55.8	0.8	2.2
08/02/2018	1550	BTMA. aDcp. DTM. Hydrophone	4	69	63.4	0.8	2.5
14/05/2018	443	BTMA. aDcp & DTM	4	79	2.2	0.9	2.7
15/05/2018	449	BTMA & aDcp	4	79	2.5	1.1	3.2

16/05/2018	547	BTMA. aDcp & DTM	3	60	6.6	1.2	4.4
17/05/2018	604	BTMA. aDcp. DTM. Hydrophone	3	60	7.2	1.2	4.4
15/04/2019	253	BTMA. aDcp & Hydrophone	3	60	22.1	0.9	3.3
16/04/2019	243	BTMA. aDcp & Hydrophone	3	60	22.1	1.1	5.1
17/04/2019	240	BTMA. aDcp & Hydrophone	3	60	24.9	1.2	3.7
18/04/2019	238	BTMA. aDcp & Hydrophone	3	58	16.4	1.0	5.3
27/05/2019	225	BTMA. aDcp. DTM. Hydrophone	1	26	34.6	1.0	4.8
29/05/2019	210	BTMA. aDcp. DTM. Hydrophone	1	28	22.0	1.1	3.3
09/12/2019	944	BTMA. aDcp. DTM. Hydrophone	2	40	29.1	0.7	2.5
10/12/2019	898	BTMA. aDcp. DTM. Hydrophone	3	60	20.1	0.6	2.5
11/12/2019	923	BTMA. aDcp. DTM. Hydrophone	3	45	34.9	0.8	2.4
12/12/2019	925	BTMA. aDcp. DTM. Hydrophone	2	37	26.4	0.7	2.7
19/12/2019	2050	BTMA. aDcp. DTM. Hydrophone	5	50	58.8	0.9	3.4
18/05/2020	514	BTMA & Hydrophone	1	57	19.7	0.9	2.8
19/05/2020	500	BTMA. aDcp & Hydrophone	2	79	30.9	1.0	2.6
20/05/2020	470	BTMA. aDcp & Hydrophone	4	40	14.5	-	-

565

566

Date	Number of DTM profiles	average interval time DTM (min)	Number of dunes	Mean H _D (m)	Mean L _D (m)	Mean C _D (m.d ⁻¹)
28/11/2016	2	18	65	0.19	2.88	43.0
29/11/2016	3	20	168	0.22	3.69	34.8
30/11/2016	3	18	121	0.24	4.16	37.6
01/12/2016	3	19	104	0.25	4.69	37.6
27/03/2017	3	38	132	0.13	3.13	28.3
28/03/2017	3	44	97	0.13	2.96	24.2
29/03/2017	3	43	117	0.14	3.25	25.7
30/03/2017	3	39	138	0.14	3.42	28.0
15/05/2017	3	65	20	0.04	2.17	18.1
16/05/2017	3	42	11	0.05	2.02	26.7
17/05/2017	3	38	18	0.05	2.01	28.0
18/05/2017	3	28	34	0.08	1.95	30.9
05/12/2017	1	73	48	0.13	2.90	17.9
06/12/2017	1	98	68	0.16	3.44	14.9
07/12/2017	1	72	63	0.17	3.62	17.3
08/12/2017	1	66	69	0.19	3.95	14.8
15/01/2018	6	23	228	0.32	6.66	38.1
16/01/2018	2	28	46	0.24	3.58	47.6
17/01/2018	3	32	52	0.25	4.36	34.9
18/01/2018	3	55	120	0.28	5.33	28.0
19/01/2018	3	31	110	0.26	4.95	31.4
30/01/2018	3	25	103	0.32	5.75	45.3
31/01/2018	4	22	83	0.28	5.02	45.4
08/02/2018	3	60	59	0.26	4.67	28.2
14/05/2018	6	35	58	0.06	2.92	20.8
16/05/2018	4	38	60	0.05	1.96	18.8
17/05/2018	6	34	81	0.05	1.98	22.3
27/05/2019	1	29	3	0.03	1.40	62.7
29/05/2019	1	26	7	0.03	1.28	30.7

09/12/2019	6	49	121	0.22	3.10	28.1
10/12/2019	6	42	227	0.17	3.60	33.2
11/12/2019	6	49	254	0.16	3.46	33.1
12/12/2019	6	50	297	0.18	3.82	35.9
19/12/2019	3	44	79	0.28	4.34	42.1

569

570

571 **Video supplement**

572 Videos of BTMA sampling were added in supplement of this manuscript to appreciate the variability of bedload in
573 the Loire River.

574 <https://doi.org/10.5446/51563>

575 <https://doi.org/10.5446/51562>

576 <https://doi.org/10.5446/51561>

577 <https://doi.org/10.5446/51560>

578 **Author contribution**

579 J. Le Guern prepared the manuscript with contributions from all co-authors. J. le Guern, T. Geay, A, Hauet, S.
580 Zanker, S. Rodrigues elaborated the experimental protocol. T. Geay developed the hydrophone signal processing
581 tools. A. Duperray P. Jugé, L. Vervynck, A. Hauet, S. Zanker, T. Geay, S. Rodrigues and J. Le Guern conducted
582 the field surveys. A. Duperray P. Jugé, and L. Vervynck performed the bathymetry post-processing. S. Rodrigues
583 and P. Tassi supervised this study. N. Claude helped in the analysis of BTMA and aDcp measurements.

584 **Competing interests**

585 The authors declare that they have no conflict of interest.

586 **Acknowledgement**

587 This study is a part of the Ph.D. thesis of the first author funded by the POI FEDER Loire (Convention no. 2017-
588 EX002207) and Agence de l'Eau Loire Bretagne (decision no.2017C005), conducted in the frame of the Masterplan
589 Plan Loire Grandeur Nature. We thank EDF DTG and ARD Intelligence des Patrimoines (Phase 2) for lending us
590 acquisition equipment. Exagone Company is acknowledged for providing us data from Teria network, Voie
591 Navigable de France (VNF) for their logistical support during field surveys and Polytech Tours. J.-P. Bakyono, P.
592 Berault, T. Bulteau, B. Deleplancouille, Y. Guerez, T. Handfus, I. Pene and C. Wintenberger, are acknowledged
593 for their help during field investigations and grain size analyses. We are grateful to T. Geay and J. Hugueny for the
594 hydrophone treatment and aDcp data post-processing tools, respectively. The authors wish to thank Pr. K. M.
595 Wantzen for checking the English quality of the manuscript.

596 **References**

- 597 Batalla, R. J.: Evaluation bed-material transport equations using field measurements in a sandy gravel-bed stream,
598 Arbúcies River, NE Spain, *Earth Surf. Process. Landforms*, 22 (2), 121-130, [https://doi.org/10.1002/\(SICI\)1096-9837\(199702\)22:2<121::AID-ESP671>3.0.CO;2-7](https://doi.org/10.1002/(SICI)1096-9837(199702)22:2<121::AID-ESP671>3.0.CO;2-7), 1997.
- 600 Banhold, K., Schüttrumpf, H., Hillebrand, G. and Frings, R.: Underestimation of sand loads during bed-load
601 measurements- a laboratory examination, in: *Proceedings of the international conference on Fluvial Hydraulics*
602 (River Flow 2016), 11-14 July 2016, Saint Louis, USA, 2406 pp., 2016.
- 603 Barton, J., Slingerland, R. R. L., Pittman, S., and Gabrielson, T. B.: Monitoring coarse bedload transport with
604 passive acoustic instrumentation: A field study, *US Geol. Surv. Sci. Investig. Rep.*, 38–51, 2010.
- 605 Bedeus, K., and Ivicsics, L.: Observation of the noise of bed load, *Gen. Assem. Comm. Hydrom. Int. Assoc. Hydrol.*
606 *Sci.* Berkeley, CA, USA, 19–31, 1963.
- 607 Bertoldi, W., Ashmore, P., and Tubino, M.: A method for estimating the mean bed load flux in braided rivers,
608 *Geomorphology*, 103, 330-340, <https://doi.org/10.1016/j.geomorph.2008.06.014>, 2009.
- 609 Best, J. L.: Sediment transport and bed morphology at river channel confluences, *Sedimentology*, 35, 481-498,
610 <https://doi.org/10.1111/j.1365-3091.1988.tb00999.x>, 1988.
- 611 Blanpain, O., Demoulin, X., Waeles, B., Ravilly, M., Garlan, T., and Guyomard, P.: Passive acoustic measurement
612 of bedload discharge features on a sandy seafloor, in: *Proceedings of Seabed and Sediment Acoustics Volume 37*
613 Part 1, Bath, United Kingdom, 7-9 september 2015.
- 614 Blott, S. J., and Pye, K.: GRADISTAT: A grain size distribution and statistics package for the analysis of
615 unconsolidated sediments, *Earth Surf. Process. Landforms*, 26 (11), 1237-1248, <https://doi.org/10.1002/esp.261>,
616 2001.
- 617 Boiten, W.: *Hydrometry*, IHE Delft Lecture Note Series, A.A. Balkema Publishers, Netherland, 256 pp,
618 <https://doi.org/10.1201/9780203971093>, 2003.
- 619 Brasington, J., Rennie, C. D., Vericat, D., Williams, R., Goodsell, B., Hicks, M., and Batalla, R.: Monitoring braided
620 river morphodynamics with an acoustic Doppler current profiler, in: *Proceedings of the 34th World Congress of the*
621 *International Association for Hydro-Environment Research and Engineering: 33rd Hydrology and Water Resources*
622 *Symposium and 10th Conference on Hydraulics in Water Engineering*, Brisbane, 3396-3403, 2011.
- 623 Carling, P. A., Williams, J. J., Götz, E., and Kelsey, A. D.: The morphodynamics of fluvial sand dunes in the River
624 Rhine, near Mainz, Germany. II. Hydrodynamics and sediment transport, *Sedimentology*, 47, 253-278,
625 <https://doi.org/10.1046/j.1365-3091.2000.00291.x>, 2000.
- 626 Church, M., and Haschenburger, J. K.: What is the “active layer”?, *Water Resour. Res.*, 53 (1), 5-10,
627 <https://doi.org/10.1002/2016WR019675>, 2017.

628 Claude, N., Rodrigues, S., Bustillo, V., Bréhéret, J. G., Macaire, J. J., and Jugé, P.: Estimating bedload transport
629 in a large sand-gravel bed river from direct sampling, dune tracking and empirical formulas, *Geomorphology*, 179,
630 40-57, <https://doi.org/10.1016/j.geomorph.2012.07.030>, 2012.

631 Claude, N., Rodrigues, S., Bustillo, V., Bréhéret, J. G., Tassi, P., and Jugé, P.: Interactions between flow structure
632 and morphodynamic of bars in a channel expansion/contraction, Loire River, France, *Water Resour. Res.*, 50,
633 <https://doi.org/10.1002/2013WR015182>, 2014.

634 Conevski, S.: Bedload Monitoring by means of Hydro-Acoustic Techniques, Ph.D. thesis, Norwegian University of
635 Science and Technology, Norway, 200 pp., 2018.

636 Conevski, S., Guerrero, M., Ruther N., and Rennie, C. D.: Laboratory investigation of apparent bedload velocity
637 measured by ADCPs under different transport conditions, *J. Hydraul. Eng.*, 145 (11),
638 [https://doi.org/10.1061/\(ASCE\)HY.1943-7900.0001632](https://doi.org/10.1061/(ASCE)HY.1943-7900.0001632), 2019.

639 Conevski, S., Guerrero, M., Winterscheid, A., Rennie, C. D., and Ruther N.: Acoustic sampling effects on bedload
640 quantification using acoustic Doppler current profilers, *Journal of Hydraulic Research*,
641 <https://doi.org/10.1080/00221686.2019.1703047>, 2020a.

642 Conevski, S., Guerrero, M., Rennie, C. D., and Ruther, N.: Towards an evaluation of bedload transport
643 characteristics by using Doppler and backscatter outputs from ADCPs, *Journal of Hydraulic Research*,
644 <https://doi.org/10.1080/00221686.2020.1818311>, 2020b.

645 Cordier, F., Tassi, P., Claude, N., Crosato, A., Rodrigues, S., and Pham Van Bang, D.: Bar pattern and sediment
646 sorting in channel contraction/expansion area: Application to the Loire River at Bréhémont (France), *Advances in*
647 *Water Resources*, 140, <https://doi.org/10.1016/j.advwatres.2020.103580>, 2020.

648 de Vries, M.: Information on the Arnhem Sampler (BTMA), Internal Report n°3-79, Delft University of Technology,
649 Department of Civil Engineering, Fluid Mechanics Group, 1979.

650 Eijkelkamp: Operating instructions: Bedload Transport Meter Arnhem, Giesbeek, Netherland, 8 pp., 2003.

651 Engel, P., and Lau, Y. L.: Computation of Bed Load Using Bathymetric Data, *Journal of the Hydraulics Division*,
652 106 (3), 369-380, 1980.

653 Folk, R. L., and Ward, W. C.: Brazos River bar (Texas); a study in the significance of grain size parameters, *Journal*
654 *of Sedimentary Research*, 27 (1), 3-26, <https://doi.org/10.1306/74D70646-2B21-11D7-8648000102C1865D>, 1957.

655 Frings, R. M., and Vollmer, S.: Guidelines for sampling bed-load transport with minimum uncertainty,
656 *Sedimentology*, 64 (6), 1630-1645, <https://doi.org/10.1111/sed.12366>, 2017.

657 Frings, R. M., Gehres, N., Promny, M., Middelkoop, H., Schüttrumpf, H., and Vollmer, S.: Today's sediment budget
658 of the Rhine River channel, focusing on the Upper Rhine Graben and Rhenish Massif, *Geomorphology*, 204, 573-
659 587, <https://doi.org/10.1016/j.geomorph.2013.08.035>, 2014.

660 Gaeuman, D., and Jacobson, R. B.: Acoustic bed velocity and bed load dynamics in a large sand bed river, *J.*
661 *Geophys. Res.*, 111, F02005, <https://doi.org/10.1029/2005JF000411>, 2006.

662 Gaeuman, D., and Jacobson, R. B.: Field Assessment of Alternative Bed-Load Transport Estimators, *J. Hydraul.*
663 *Eng.*, 133 (12), 1319-1328, [https://doi.org/10.1061/\(ASCE\)0733-9429\(2007\)133:12\(1319\)](https://doi.org/10.1061/(ASCE)0733-9429(2007)133:12(1319)), 2007.

664 Gaeuman, D., and Pittman, S.: Relative Contributions of Sand and Gravel Bedload Transport to Acoustic Doppler
665 Bed-Velocity Magnitudes in the Trinity River, California, U.S. Geological Survey Scientific Investigations Report,
666 2010-5091, 2010.

667 Gaweesh, M. T. K., and van Rijn, L. C.: Bed-load sampling in sand-bed rivers, *J. Hydraul. Eng.*, 120 (12), 1364-
668 1384, [https://doi.org/10.1061/\(ASCE\)0733-9429\(1994\)120:12\(1364\)](https://doi.org/10.1061/(ASCE)0733-9429(1994)120:12(1364)), 1994.

669 Geay, T., Belleudy, P., Gervaise, C., Habersack, H., Aigner, J., Kreisler, A., Seitz, H., and Laronne, J. B.: Passive
670 acoustic monitoring of bed load discharge in a large gravel bed river, *J. Geophys. Res.: Earth Surf.*, 122 (2),
671 <https://doi.org/10.1002/2016JF004112>, 2017.

672 Geay, T., Michel, L., Zanker, S., and Rigby, J. R.: Acoustic wave propagation in rivers: an experimental study. *Earth*
673 *Surface Dynamics*, 7 (2), 537–548, <https://doi.org/10.5194/esurf-7-537-2019>, 2019.

674 Geay, T., Zanker, S., Misset, C., and Recking, A.: Passive Acoustic Measurement of Bedload Transport: Toward
675 a Global Calibration Curve?, *J. Geophys. Res.: Earth Surf.*, 125 (8), <https://doi.org/10.1029/2019JF005242>, 2020.

676 Gimbert, F., Fuller, B. M., Lamb, M. P., Tsai, V. C., and Johnson, J. P. L.: Particle transport mechanics and induced
677 seismic noise in steep flume experiments with accelerometer-embedded tracers, *Earth Surf. Process. Landforms*,
678 44, 219-241, <https://doi.org/10.1002/esp.4495>, 2019.

679 Gray, J. R., Gartner, J. W., Barton, J. S., Gaskin, J., Pittman, S. A., and Rennie, C. D.: Surrogate Technologies for
680 Monitoring Bed-Load Transport in Rivers, *Sedimentology of Aqueous Systems*, 46-79,
681 <https://doi.org/10.1002/9781444317114.ch2>, 2010.

682 Grill, G., Lehner, B., Thieme, M. et al.: Mapping the world's free-flowing rivers. *Nature* 569, 215–221,
683 <https://doi.org/10.1038/s41586-019-1111-9>, 2019.

684 Hilldale, R. C., Goodwiller, B. T., Carpenter, W. O., and Chambers, J. P.: Measuring Coarse Bed Load Using
685 Hydrophones, Closeout report, Reclamation Managing Water in the West, 2014.

686 Holmes, R. R. Jr.: Measurement of Bedload Transport in Sand-Bed Rivers: A Look at Two Indirect Sampling
687 Methods, U.S. Geological Survey Scientific Investigations Report, 2010-5091, 2010.

688 Jackson, R. G.: Hierarchical attributes and a unifying model of bed forms composed of cohesionless material and
689 produced by shearing flow, *Geological Society of America Bulletin*, 86, 1523-1533, 1975.

690 Jamieson, E. C., Rennie, C. D., Jacobson, R. B., and Townsend, R. D.: Evaluation of ADCP Apparent Bed Load
691 Velocity in a large Sand-Bed River: Moving versus Stationary Boat Conditions, *J. Hydraul. Eng.*, 137, 1064-1071,
692 [https://doi.org/10.1061/\(ASCE\)HY.1943-7900.0000373](https://doi.org/10.1061/(ASCE)HY.1943-7900.0000373), 2011.

693 Kenney, T. A. (2006), Cross-sectional progression of apparent bedload velocities, in: Proceedings of the Eighth
694 Federal Interagency Sedimentation Conference (8th FISC), April 2–6 2006, Reno, Nevada, USA, 8 pp., 2006.

695 Kondolf, G. M., Schmitt, R. J. P., Carling, P., et al.: Changing sediment budget of the Mekong: Cumulative threats
696 and management strategies for a large river basin. *Sci Total Environ.*, 625, 114-134,
697 <https://doi.org/10.1016/j.scitotenv.2017.11.361>, 2018.

698 Kostaschuk, R., and Villard, P.: Flow and sediment transport over large subaqueous dunes: Fraser River, Canada,
699 *Sedimentology*, 43 (5), 849-863, <https://doi.org/10.1111/j.1365-3091.1996.tb01506.x>, 1996.

700 Kostaschuk, R., Best, J., Villard, P., Peakall, J., and Franklin, M.: Measuring flow velocity and sediment transport
701 with an acoustic Doppler current profiler, *Geomorphology*, 68, 25-37,
702 <https://doi.org/10.1016/j.geomorph.2004.07.012>, 2005.

703 Latosinski, F. G., Szupiany, R. N., Guerrero, M., Amsler, M. L., and Vionnet, C.: The ADCP's bottom track capability
704 for bedload prediction: Evidence on method reliability from sandy river applications, *Flow Measurement and*
705 *Instrumentation*, 54, 124-135, <https://doi.org/10.1016/j.flowmeasinst.2017.01.005>, 2017.

706 Leary, K. C. P., and Buscombe, D.: Estimating sand bed load in rivers by tracking dunes: a comparison of methods
707 based on bed elevation time series, *Earth Surf. Dynam.*, 8, 161-172, <https://doi.org/10.5194/esurf-8-161-2020>,
708 2020.

709 Le Guern, J., Rodrigues, S., Tassi, P., Jugé, P., Handfus, T., Duperray, A., and Berrault, P.: Influence of migrating
710 bars on dune geometry, in: *Book of Abstracts of the 6th Marine and River Dune Dynamics conference*, 1-3 April
711 2019, Bremen, Germany, 157-160, 2019a.

712 Le Guern, J., Rodrigues, S., Tassi, P., Jugé, P., Handfus, T., and Duperray, A.: Initiation, growth and interactions
713 of bars in a sandy-gravel bed river, in: *Book of Abstracts of the 11th Symposium on River, Coastal and Estuarine*
714 *Morphodynamics*, 16-21 November 2019, Auckland, New-Zealand, 226 pp., 2019b.

715 Marineau, M. D., Wright, S. A., and Gaeuman, D.: Calibration of sediment-generated noise measured using
716 hydrophones to bedload transport in the Trinity River, California, USA, in: *Proceeding of River Flow 2016 - eighth*
717 *International Conference on Fluvial Hydraulics*, Saint Louis, USA, 12-15 July 2016, 1519–1526, 2016.

718 Mendoza, A., Abad, J. D., Langendoen, E. J., Wang, D., Tassi, P., and El Kadi Abderrezzak, K.: Effect of Sediment
719 Transport Boundary conditions on the Numerical Modeling of Bed Morphodynamics, *J. Hydraul. Eng.*, 143 (4),
720 [https://doi.org/10.1061/\(ASCE\)HY.1943-7900.0001208](https://doi.org/10.1061/(ASCE)HY.1943-7900.0001208), 2017.

721 Nittrouer, J. A., Allison, M. A., and Campanella, R.: Bedform transport rates for the lowermost Mississippi River, *J.*
722 *Geophys. Res.*, 113, F03004, <https://doi.org/10.1029/2007JF000795>, 2008.

723 Peters, J. J.: Discharge and Sand Transport in the Braided Zone of the Zaire Estuary, *Netherlands Journal of Sea*
724 *Research*, 12, 273-292, [https://doi.org/10.1016/0077-7579\(78\)90031-5](https://doi.org/10.1016/0077-7579(78)90031-5), 1978.

725 Ramoos, R., and Rennie, C. D.: Laboratory Measurement of Bedload with an ADCP, U.S. Geological Survey
726 Scientific Investigations Report, 2010-5091, 2010.

727 Reesink, A. J. H., Parsons, D. R., and Thomas, R. E.: Sediment transport and bedform development in the lee of
728 bars: Evidence from fixed- and partially-fixed bed experiments, in: Proceeding of River Flow 2014 - seventh
729 International Conference on Fluvial Hydraulics, Lausanne, Switzerland, 3-5 Septembre 2014, 8 pp., 2014.

730 Rennie, C. D., and Millar, R. G.: Measurement of the spatial distribution of fluvial bedload transport velocity in both
731 sand and gravel, *Earth Surf. Process. Landforms*, 29, 1173-1193, doi:10.1002/esp.1074, 2004.

732 Rennie, C. D., and Villard, P. V.: Site specificity of bed load measurement using an acoustic Doppler current profiler,
733 *J. Geophys. Res.*, 109, F03003, <https://doi.org/10.1029/2003JF000106>, 2004.

734 Rennie, C. D., Millar, R. G., and Church, M. A.: Measurement of Bed Load Velocity using an Acoustic Doppler
735 Current Profiler, *J. Hydraul. Eng.*, 128 (5), 473-483, [https://doi.org/10.1061/\(ASCE\)0733-9429\(2002\)128:5\(473\)](https://doi.org/10.1061/(ASCE)0733-9429(2002)128:5(473)),
736 2002.

737 Rennie, C. D., Vericat, D., Williams, R. D., Brasington, J., and Hicks, M.: Calibration of acoustic doppler current
738 profiler apparent bedload velocity to bedload transport rate, in: *Gravel-Bed Rivers: Processes and Disasters*,
739 Oxford, UK: Wiley Blackwell, 209–233, <https://doi.org/10.1002/9781118971437.ch8>, 2017.

740 Rodrigues, S., Mosselman, E., Claude, N., Wintenberger, C. L., and Jugé, P.: Alternate bars in a sandy gravel bed
741 river: generation, migration and interactions with superimposed dunes, *Earth Surf. Process. Landforms*, 40 (5),
742 610-628, <https://doi.org/10.1002/esp.3657>, 2015.

743 Simons, D. B., Richardson, E. V., and Nordin, C. F. Jr.: Bedload Equation for Ripples and Dunes, U.S. Geol. Survey
744 Prof. Paper, 462-H, <https://doi.org/10.3133/pp462H>, 1965.

745 Syvitski, J. P. M., and Milliman, J. D.: Geology, Geography, and Humans Battle for Dominance over the Delivery of
746 Fluvial Sediment to the Coastal Ocean, *The Journal of Geology*, 15(1), 1-19, <https://doi.org/10.1086/509246>, 2007.

747 Ten Brinke, W. B. M., Wilbers, A. W. E., and Wesseling, C.: Dune growth, decay and migration rates during a large-
748 magnitude flood at a sand and mixed sand-gravel bed in the Dutch Rhine river system, in: *In Fluvial Sedimentology*
749 VI, Vol. 28 of Special Publications of the International Association of Sedimentologists, 15-32,
750 <https://doi.org/10.1002/9781444304213.ch2>, 1999.

751 Thorne, P. D., Heathershaw, A. D., and Troiano, L.: Acoustic Detection of Seabed Gravel Movement in Turbulent
752 Tidal Currents, *Marine Geology*, 54, M43-M48, [https://doi.org/10.1016/0025-3227\(84\)90035-5](https://doi.org/10.1016/0025-3227(84)90035-5), 1984.

753 Thorne, P. D.: The measurement of acoustic noise generated by moving artificial sediments, *J. Acoust. Soc. Am.*,
754 78 (3), 1013–1023, <https://doi.org/10.1121/1.393018>, 1985.

755 Thorne, P. D.: Laboratory and marine measurements on the acoustic detection of sediment transport, *J. Acoust.*
756 *Soc. Am.*, 80(3), 899, <https://doi.org/10.1121/1.393913>, 1986.

757 Thorne, P. D.: An overview of underwater sound generated by interparticle collisions and its application to the
758 measurements of coarse sediment bedload transport, *Earth Surf. Dyn.*, 2 (2), 531–543,
759 <https://doi.org/10.5194/esurf-2-531-2014>, 2014.

760 Van den Berg, J. H.: Bedform migration and bed-load transport in some rivers and tidal environments,
761 Sedimentology, 34, 681-698, <https://doi.org/10.1111/j.1365-3091.1987.tb00794.x>, 1987.

762 Van der Mark, C. F., and Blom, A.: A new and widely applicable tool for determining the geometric properties of
763 bedforms, Civil Engineering & Management Research Report 2007R-003/WEM-002 ISSN 1568-4652, University
764 of Twente, Enschede, Netherlands, 57 pp., 2007.

765 Van Rijn, L. C.: Sediment Transport. Part I: Bed Load Transport, J. Hydraul. Eng., 110, 1431-1456,
766 [https://doi.org/10.1061/\(ASCE\)0733-9429\(1984\)110:10\(1431\)](https://doi.org/10.1061/(ASCE)0733-9429(1984)110:10(1431)), 1984.

767 Van Rijn, L. C., and Gaweesh, M. T. K.: New Total Sediment-Load Sampler, J. Hydraul. Eng., 118 (12), 1686–
768 1691. [https://10.1061/\(ASCE\)0733-9429\(1992\)118:12\(1686\)](https://10.1061/(ASCE)0733-9429(1992)118:12(1686)), 1992.

769

770 Villard, P. V., and Church, M.: Bar and dune development during a freshet: Fraser River Estuary, British Columbia,
771 Canada, Sedimentology, 52, 737-756, <https://doi.org/10.1111/j.1365-3091.2005.00721.x>, 2005.

772 Villard, P., Church, M., and Kostaschuk, R.: Estimating bedload in sand-bed channels using bottom tracking from
773 an acoustic Doppler profiler, Spec. Publs int. Ass. Sediment, 35, 197-209,
774 <https://doi.org/10.1002/9781444304350.ch12>, 2005.

775 Vörösmarty, C., McIntyre, P., Gessner, M., Dudgeon, D., Prusevich, A., Green, P., Glidden, S., Bunn, S. E.,
776 Sullivan, C. A., Reidy Liermann, C., and Davies, P. M.: Global threats to human water security and river biodiversity,
777 Nature, 467, 555–561, <https://doi.org/10.1038/nature09440>, 2010.

778 Wilbers, A.: The development and hydraulic roughness of subaqueous dunes, Neth. Geogr. Stud, Fac. of Geosci.,
779 Utrecht Univ., Utrecht, Netherlands. 323, 224 pp., 2004.

780 Williams, R. D., Rennie, C. D., Brasington, J., Hicks, D. M., and Vericat, D.: Linking the spatial distribution of bed
781 load transport to morphological change during high-flow events in shallow braided river, J. Geophys. Res. Earth
782 Surf., 120, 604–622, <https://doi.org/10.1002/2014JF003346>, 2015.